

Magnetic Electron Scattering from Nuclei

J. GOLDEMBERG

École Normale Supérieure, Laboratoire de l'Accélérateur Linéaire, Orsay (78), France

R. H. PRATT

Department of Physics, University of Pittsburgh, Pittsburgh, Pennsylvania

In this article we review the calculations and experimental information available in the studies of electron scattering (elastic and inelastic) from the magnetic-moment distribution of nuclei. The corresponding information on the properties of nucleons has been reviewed previously and is not discussed here. As usual in electron-scattering investigations we are concerned mostly with the determination of two functions of the momentum transfer, the charge and magnetic form factors or linear combinations of them, which are closely related to the spatial structure of the charge and magnetic-moment distributions. We specialize the discussion to the magnetic form factor and the nuclear properties connected with it.

I. Introduction.....	311
II. Structure of Cross Sections for Electron Scattering from Nuclear Targets.....	311
A. General Form.....	311
B. Proof.....	312
C. Interpretation.....	313
D. Connection with Photoabsorption.....	313
E. Extensions and Limitations.....	314
F. The Measurement of Magnetic Scattering.....	314
III. Extracting Information on Nuclear Structure.....	316
A. Bremsstrahlung at Large Angles.....	316
B. Radiative Corrections.....	319
IV. Interpreting Information on Nuclear Structure.....	319
A. General Remarks.....	319
B. Elastic Scattering.....	321
1. The Deuteron.....	322
2. H ³ and He ³	323
3. He ⁴	323
4. F ¹⁹	324
C. Inelastic Scattering in Levels.....	324
1. M1 Levels.....	325
2. E1 Levels.....	326
D. Quasielastic (Incoherent) Scattering.....	328

I. INTRODUCTION

In this article we review the calculations and experimental information available in the studies of electron scattering (elastic and inelastic) from the magnetic-moment distribution of nuclei. The corresponding information on the properties of nucleons has been reviewed previously (Refs. 1-3) and is not discussed here. As usual in electron-scattering investigations we are concerned mostly with the determination of two functions of the momentum transfer, the charge and magnetic form factors or linear combinations of them, which are closely related to the spatial structure of the charge and magnetic-moment distributions. We specialize the discussion to the magnetic form factor and the nuclear properties connected with it.

In Sec. II we discuss the general structure of scattering formulas and methods of measuring the magnetic cross

¹ R. Hofstadter, *Ann. Rev. Nucl. Sci.* **7**, 231 (1957).

² R. Hofstadter, *Electron Scattering and Nuclear and Nucleon Structure*, a collection of reprints with an introduction (W. A. Benjamin, Inc., New York, 1963); R. Herman and R. Hofstadter, *High Energy Electron Scattering Tables* (Stanford University Press, Stanford, 1960). See also, T. A. Griffy and L. I. Schiff, "Electromagnetic Form Factors," to be published in the book *High Energy Physics*.

³ L. N. Hand, D. G. Miller, and R. Wilson, *Rev. Mod. Phys.* **35**, 335 (1963).

section. The approximations of the theory and possible extensions are discussed briefly. In Sec. III methods of extracting information on nuclear structure are presented ("radiation tail" problems). In Sec. IV the connection between the information extracted in Sec. III and the nuclear properties (such as nuclear currents, nuclear magnetization, and exchange currents) are discussed separately for elastic, inelastic, and quasi-elastic scattering.⁴

II. STRUCTURE OF CROSS SECTIONS FOR ELECTRON SCATTERING FROM NUCLEAR TARGETS

A. General Form

For any process in which a single (virtual) photon interacts with a nucleus, as in the electron-nucleus scattering diagram of Fig. 1, the entire dependence of the cross section on nuclear properties can be described by two form factors, W_1 and W_2 , which are functions of the invariant momentum transfer q^2 and the energy transfer⁵ (or of q^2 and $q \cdot P$). This follows from the vector nature of the photons and electromagnetic current conservation; it also assumes an experimental situation in which the target is initially unoriented and all final nuclear states P' consistent with specified P , q are summed over (i.e., in the electron scattering process of Fig. 1 only the final electron p' would be detected).

Further, neglecting the mass of the electron, the cross section for electron scattering from a nuclear target can be given explicitly in the laboratory frame in terms of these form factors as⁶

$$\frac{d\sigma}{d\Omega'de'} = \frac{4Z^2\alpha^2}{q^4} \frac{\epsilon'^2}{M_T} \cos^2 \frac{1}{2}\theta [W_2 + 2W_1 \tan^2 \frac{1}{2}\theta], \quad (1)$$

where θ is the scattering angle, M_T the mass of the

⁴ For a more detailed review of nuclear structure and inelastic electron scattering see T. de Forest and J. D. Walecka, *Advan. Phys.* (to be published).

⁵ S. D. Drell and J. D. Walecka, *Ann. Phys. (N.Y.)* **28**, 18 (1964).

⁶ We use the notation $\hbar=c=m=1$, with m the rest mass of the electron.

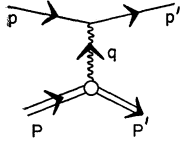


FIG. 1. Diagram for an electron-nucleus interaction. p and p' are the initial and final momentum of the electron, P and P' the initial and final momentum of the nucleus, and q the momentum transfer.

target, ϵ and ϵ' the initial and final electron energies, and the 4-momentum transfer $q^2=4\epsilon\epsilon'\sin^2\frac{1}{2}\theta$, $q\cdot P=M_T(\epsilon-\epsilon')$. The objective of such experiments is the determination of these form factors, W_1 and W_2 , and their theoretical interpretation in terms of nuclear models.

If one does not neglect the electron mass, the factors that multiply the form factors in Eq. (1) become slightly more complicated (see below). If one considers a process in which the electron lines of Fig. 1 may be virtual, as in bremsstrahlung or pair production, the factors become appreciably more complex (Sec. IIIA), but the cross section is still of the form AW_1+BW_2 , where the factors A and B can be given explicitly and all information on nuclear structure continues to reside in W_1 and W_2 . Equation (1) is equally applicable to electron, positron, and muon scattering from a nucleus; for a given nucleus the *same* form factors W_1 and W_2 should be used in all three cases.

B. Proof

For completeness we indicate here the proof of the foregoing statements, following the treatment of Drell and Walecka.⁵ We adopt the following notations⁷: P denotes the initial 4-momentum of the target, $P^2=-M_T^2$. q is the 4-momentum of the virtual photon, and $P'=P+q$ is the final 4-momentum of the target. We assume that the target is initially unoriented and that experimentally *all final nuclear states* consistent with the given kinematic conditions (given q and P) are summed over. In this case, the contribution of the nuclear part of the process indicated in Fig. 1 is given by

$$W_{\mu\nu} = \frac{(2\pi)^3\Omega}{(Ze)^2} \sum_{\text{initial states}} \sum_{\text{final states}} \delta^{(4)}(P-P'+q) \langle P | J_\nu(0) | P' \rangle \times \langle P' | J_\mu(0) | P \rangle (E), \quad (2)$$

where Ω is the normalization volume, E is the initial energy of the target, $\bar{\Sigma}$ indicates an average over the initial target states (i.e., M_T of the target), $|P\rangle$ and $|P'\rangle$ are the Heisenberg state vectors of the initial and final nuclear states (that is they are eigenstates of the nuclear 4-momentum operator P_μ), and $J_\mu(0)$ is the electromagnetic current operator of the nucleus at the space-time point $x_\mu=0$. The four-dimensional delta function summarizes the translation invariance of the theory. Lorentz invariance tells us that $W_{\mu\nu}$ must be a second-rank tensor since the current operator is a 4-vector. Because of the sum over initial and final

states, there are only two 4-vectors on which this tensor can depend, P and q . Since $P^2=-M_T^2$, there are only two independent scalars which can be formed from these 4-vectors, q^2 and $q\cdot P$. Thus the most general form of the tensor $W_{\mu\nu}$ is

$$W_{\mu\nu} = A(q^2, q\cdot P)\delta_{\mu\nu} + B(q^2, q\cdot P)q_\mu q_\nu + C(q^2, q\cdot P)P_\mu P_\nu + D(q^2, q\cdot P)(q_\mu P_\nu + q_\nu P_\mu) + E(q^2, q\cdot P)(q_\mu P_\nu - q_\nu P_\mu). \quad (3)$$

No term in $\epsilon_{\mu\nu\rho\sigma}P_\rho q_\sigma$ can appear since the current operator is a polar vector under spatial reflections. We know further that the nuclear current operator must satisfy the continuity equation

$$(\partial/\partial x_\mu)J_\mu(x) = 0, \quad (4)$$

which implies that $q_\mu W_{\mu\nu} = W_{\mu\nu} q_\nu = 0$. These relations are sufficient to eliminate three of the invariant functions and one can thus write a symmetric tensor, with W_1 and W_2 both ≥ 0 according to the definition in Eq. (1)

$$W_{\mu\nu} = W_1(q^2, q\cdot P)\left(\delta_{\mu\nu} - \frac{q_\mu q_\nu}{q^2}\right) + W_2(q^2, q\cdot P)\frac{1}{M_T^2}\left(P_\mu - \frac{P\cdot q}{q^2}q_\mu\right)\left(P_\nu - \frac{P\cdot q}{q^2}q_\nu\right). \quad (5)$$

This theorem is due to Bjorken,⁸ von Gehlen,⁹ and Gourdin.¹⁰

In terms of W_1 and W_2 the electron or muon scattering cross section for fixed electron energy and angle but summing over all else can be computed in standard fashion:

$$d\sigma = 2Z^2\alpha^2 \frac{d^3\mathbf{p}'}{2\epsilon' q^4} W_{\mu\nu} N_{\mu\nu} \frac{1}{[(\mathbf{p}\cdot P)^2 - m^2 M_T^2]^{\frac{1}{2}}}, \quad (6)$$

where

$$N_{\mu\nu} = -\frac{1}{2} \text{Tr} \gamma_\mu(m - i\boldsymbol{\gamma}\cdot\mathbf{p})\gamma_\nu(m - i\boldsymbol{\gamma}\cdot\mathbf{p}') = 2[\mathbf{p}_\mu\mathbf{p}'_\nu + \mathbf{p}'_\nu\mathbf{p}_\mu - \delta_{\mu\nu}(\mathbf{p}\cdot\mathbf{p}'+m^2)]. \quad (7)$$

Combining gives

$$d\sigma = 2Z^2\alpha^2 \frac{d^3\mathbf{p}'}{2\epsilon' q^4} \frac{1}{[(\mathbf{p}\cdot P)^2 - m^2 M_T^2]^{\frac{1}{2}}} \times \left\{ 2(q^2 - 2m^2)W_1 + 2\left[\frac{2(\mathbf{p}\cdot P)[(\mathbf{p}-q)\cdot P]}{M_T^2} - \frac{1}{2}q^2\right]W_2 \right\}. \quad (8)$$

The three independent scalar functions in electron scattering can be taken as ϵ , ϵ' , θ in the laboratory system or as the three scalar variables q^2 , $\mathbf{p}\cdot P$, and $q\cdot P$. Measurements at fixed q^2 and $q\cdot P$ can separate W_1 and W_2 and check the one-photon-exchange form.

⁸ J. D. Bjorken (unpublished).

⁹ R. von Gehlen, Phys. Rev. **118**, 1455 (1960).

¹⁰ M. Gourdin, Nuovo Cimento **21**, 1094 (1961).

⁷ We use a metric such that $a_\mu = (\mathbf{a}, ia_0)$ and $\mathbf{a}\cdot\mathbf{b} = \mathbf{a}\cdot\mathbf{b} - a_0b_0$. In this metric $q^2 > 0$ for both scattering and pair production.

The cross section can be written in the laboratory frame as

$$\frac{d\sigma}{d\Omega'd|\mathbf{p}'|} = \frac{2Z^2\alpha^2}{q^4} \left(\frac{\mathbf{p}'^2}{|\mathbf{p}'|} \right) \frac{1}{M_T} \\ \times [2(\epsilon\epsilon' - |\mathbf{p}||\mathbf{p}'|\cos\theta - 2m^2)W_1 \\ + (\epsilon\epsilon' + |\mathbf{p}||\mathbf{p}'|\cos\theta + m^2)W_2],$$

where

$$-q \cdot P/M_T = \epsilon - \epsilon', \\ q^2 = 2\epsilon\epsilon' - 2|\mathbf{p}||\mathbf{p}'|\cos\theta - 2m^2. \quad (9)$$

These formulas simplify if one can neglect the mass of the electron

$$\frac{d\sigma}{d\Omega'd\epsilon'} = \frac{4Z^2\alpha^2}{q^4} \frac{\epsilon'^2}{M_T} \cos^2 \frac{1}{2}\theta \\ \times [W_2(q^2, q \cdot P) + 2W_1(q^2, q \cdot P) \tan^2 \frac{1}{2}\theta], \\ q^2 = 4\epsilon\epsilon' \sin^2 \frac{1}{2}\theta. \quad (10)$$

C. Interpretation

Considering the electron-nucleus scattering cross section as a function of q^2 , $q \cdot P$, and θ , it is clear that for fixed energy and momentum transfer to the nucleus an experiment at small electron-scattering angles is sensitive to the form factor W_2 and an experiment at large scattering angles is sensitive to W_1 . Theoretical predictions for these form factors depend on a model for the nucleus. However, it is easy to see that W_1 , measurable at large angles, is connected with the magnetic properties of the nucleus. Thus, in the case that we have only elastic scattering from the nucleus, $P'^2 = -M_T^2$ and $2q \cdot P = q^2$, and a spin-zero target we have with the aid of Eq. (4)

$$(\Omega^2 EE')^{\frac{1}{2}} \langle P' = p + q | J_\mu(0) / Ze | P \rangle \\ = F(q^2) [P_\mu - (P \cdot q / q^2) q_\mu] \quad (11)$$

with $F(0) = 1$. By substituting in the equation for $W_{\mu\nu}$ one finds

$$W_1 = 0, \\ W_2 = |F(q^2)|^2 (M_T^2 / E') \delta(E - E' - q_0), \quad (12)$$

i.e., for a spin-zero nucleus (no magnetic moment) W_1 vanishes for elastic scattering. Similarly (Sec. IVA) one can show in the elastic scattering from a fixed nucleus that, for small momentum transfer q^2 , W_1 is proportional to the magnetic moment of the nucleus. In elastic scattering from a fixed nucleus $F(q^2)$ is simply the Fourier transform of the charge distribution of the nucleus.

The Rosenbluth cross section for elastic scattering from a spin- $\frac{1}{2}$ target is also a special case of Eq. (9)

$$(\Omega^2 EE')^{\frac{1}{2}} \langle P', \lambda' | J_\mu(0) / Ze | P, \lambda \rangle \\ = iM_T \bar{u}_{\lambda'}(\mathbf{p}') [F_1(q^2)\gamma_\mu + F_2(q^2)\sigma_{\mu\nu}q_\nu] u_\lambda(\mathbf{p}) \quad (13)$$

in the usual Dirac notation with $F_1(0) = 1$, $F_2(0) = \frac{1}{2}\lambda/M_T$ the anomalous magnetic moment. Inserting this in the equation for $W_{\mu\nu}$ one finds

$$W_1 = q^2 | \frac{1}{2} F_1(q^2) + M_T F_2(q^2) |^2 \delta(E - E' - q_0) (E')^{-1}, \quad (14)$$

$$W_2 = M_T^2 [|F_1(q^2)|^2 + q^2 |F_2(q^2)|^2] \delta(E - E' - q_0) (E')^{-1}. \quad (15)$$

Inserting in Eq. (9) yields (integrating over ϵ')

$$\frac{d\sigma}{d\Omega'} = \frac{Z^2\alpha^2}{4\epsilon^2 \sin^4 \frac{1}{2}\theta} \cos^2 \frac{1}{2}\theta \left[\frac{1}{1 + (2\epsilon/M_T) \sin^2 \frac{1}{2}\theta} \right] \\ \times \{ [|F_1|^2 + q^2 |F_2|^2] \\ + (q^2/2M_T^2) |F_1 + 2M_T F_2|^2 \tan^2 \frac{1}{2}\theta \}, \quad (16)$$

which is the Rosenbluth result.¹¹

Another method of analysis of electron scattering involves the separation of the cross section into contributions from longitudinal and transverse currents.¹² From $q_\mu W_{\mu\nu} = W_{\mu\nu} q_\nu = 0$ and the similar relation for $N_{\mu\nu}$ one can eliminate all scalar terms in $N_{\mu\nu} W_{\mu\nu}$. In the laboratory frame there is no interference between longitudinal terms (along \mathbf{q}) and transverse terms:

$$N_{\mu\nu} W_{\mu\nu} = [1 - (q_3/q_0)^2]^2 N_{33} W_{33} + N_{tt} W_{tt}. \quad (17)$$

D. Connection with Photoabsorption

If the photon of Fig. 1 were real (and we dispense with the electron) we would be concerned with the total cross section σ_γ for absorption of a real photon. Our previous analysis of $W_{\mu\nu}$ in terms of form factors W_1 and W_2 would still be valid, except that here we would now have the condition $q^2 = 0$. The cross section is

$$\sigma_\gamma = \{ (2\pi)^2 Z^2 \alpha [(q \cdot P)^2]^{-\frac{1}{2}} \} \frac{1}{2} W_{\mu\mu} |_{q^2=0}. \quad (18)$$

We can thus relate W_1 and W_2 evaluated at $q^2 = 0$ to σ_γ .

The expression Eq. (5) for $W_{\mu\nu}$ has no singularities when one sets $q^2 = 0$, as can be seen from Eq. (2), since the matrix elements are just the physical amplitudes for photoabsorption to individual final states. The apparent singularities in Eq. (5) hence must cancel as $q^2 \rightarrow 0$, whence one deduces

$$W_2 = O(q^2), \quad W_1 - [(P \cdot q)^2 / q^2] W_2 = O(q^2); \\ (W_{\mu\mu} = 2W_1)_{q^2=0} \quad (19)$$

and hence

$$\sigma_\gamma = \{ (2\pi)^2 Z^2 \alpha [(q \cdot P)^2]^{-\frac{1}{2}} \} W_1 |_{q^2=0}. \quad (20)$$

For fixed energy transfer and small q^2 we can thus write the form factors W_1 and W_2 for electron-nucleus scattering in terms of the total photoabsorption cross section at the same energy transfer as

$$W_1 = [(2\pi)^2 Z^2 \alpha]^{-1} [(q \cdot P)^2]^{\frac{1}{2}} \sigma_\gamma, \\ W_2 = [(2\pi)^2 Z^2 \alpha]^{-1} \{ q^2 [(q \cdot P)^2]^{-\frac{1}{2}} \} \sigma_\gamma. \quad (21)$$

¹¹ M. N. Rosenbluth, Phys. Rev. **79**, 615 (1950).

¹² R. H. Dalitz and D. Yennie, Phys. Rev. **105**, 1598 (1957).

E. Extensions and Limitations

From the derivation of the form for $W_{\mu\nu}$ it is apparent where the assumption of an experimental situation appropriate to an average over initial and a sum over final nuclear states enters: without these requirements there would be more independent 4-vectors on which the tensor $W_{\mu\nu}$ could depend and consequently more independent form factors. Hence one can expect to measure additional nuclear properties, (1) by polarizing or aligning the target, or (2) by measuring independent properties of the nuclear final state in addition to detecting the electron. Effects of nuclear orientation have been discussed recently by Wiegert and Rose¹³; some general results for the amplitudes for two- and three-body final states have been given by Berman.¹⁴

On the other hand, the entire method of analysis we have presented depends on the assumption of one-photon exchange only; this corresponds to neglecting higher Born-approximation corrections of $O(Z\alpha)$ and can only be appropriate for light nuclei. Deviations from Born approximation (one-photon exchange) can be tested by observing differences between electron and positron scattering cross sections, or by detecting violation of the two form-factor parameterization of electron scattering. Experimental results on the difference between electron and positron scattering from nuclei at small angles, both elastic and inelastic, have been obtained by Goldemberg, Pine, and Yount.¹⁵ When many-photon exchange effects must be considered, no correspondingly simple theoretical analysis of experimental results has yet been developed. Three approaches have been used in calculation of both elastic and inelastic scattering: (1) Second Born approximation,¹⁶ (2) numerical partial-wave calculations for scattering in a potential,¹⁷ and (3) replacement of the free electron of Fig. 1 with a modified plane wave.¹⁸ When applied to inelastic scattering these methods generally correspond to the use of a distorted-wave Born approximation in Fig. 1: the excitation of the nucleus treated only in lowest order, but the incoming and outgoing wave function treated more exactly. Both theory and experiment agree that in light nuclei for small momentum transfers (within the first zero of the form factors) the one-photon exchange analysis is adequate.

¹³ L. J. Wiegert and M. E. Rose, Nucl. Phys. **51**, 529 (1964); D. Schildknecht, Phys. Letters **10**, 254 (1964). Some time ago R. G. Newton [Phys. Rev. **103**, 385 (1956); **109**, 2213 (1958); and **110**, 1483 (1958)] discussed the use of electron scattering for aligned nuclei for obtaining information on magnetic moment distributions.

¹⁴ S. M. Berman, Phys. Rev. **135**, B1249 (1964).

¹⁵ J. Goldemberg, J. Pine, and D. Yount, Phys. Rev. **132**, 406 (1953).

¹⁶ S. D. Drell and R. H. Pratt, Phys. Rev. **125**, 1394 (1962).

¹⁷ T. A. Griffy, D. S. Onley, J. T. Reynolds, and L. C. Biedenharn, Phys. Rev. **128**, 833 (1962); D. S. Onley, T. A. Griffy, and J. T. Reynolds, *ibid.* **129**, 1689 (1963); D. S. Onley, J. T. Reynolds, and L. E. Wright, *ibid.* **134**, B945 (1964).

¹⁸ D. R. Yennie, F. L. Boos, Jr., and D. G. Ravenhall, Phys. Rev. **137**, B882 (1965); A. Baker, Phys. Rev. **134**, B240 (1964); H. Greenstein (to be published).

F. The Measurement of Magnetic Scattering

As seen above [Eq. (10)] all the processes considered in this paper have a differential cross section which can be written in the form

$$d\sigma/d\Omega = \sigma_{NS}[A(q) + B(q) \tan^2 \frac{1}{2}\theta],$$

$$\sigma_{NS} = \left(\frac{Z\alpha}{2\epsilon}\right)^2 \frac{\cos^2 \theta}{\sin^4 \frac{1}{2}\theta} \frac{E}{E'}, \quad (22)$$

where $A(q)$ and $B(q)$ are functions of the momentum and energy transfer, related to the charge and magnetic form factors. Consequently if one has two measurements of $d\sigma/d\Omega$ at two angles but at the same momentum and energy transfer, one can obtain $A(q)$ and $B(q)$. Better yet, in a linear plot of $d\sigma/d\Omega \sigma_{NS}$ as ordinate against $\tan^2 \frac{1}{2}\theta$ as abscissa, $A(q)$ is the intercept with the ordinate axis and $B(q)$ the slope of the resulting straight line. An example is shown in Fig. 2. If the magnetic contribution to the scattering is not insignificant compared to the charge scattering, this method permits the determination of F_{mag} with a precision comparable to F_{ch} .

The relative order of the magnetic to charge elastic-scattering cross sections, for example, can be simply estimated as the ratio of the strength of the magnetic $q\mu$ and Coulomb interactions eZ

$$\left(\frac{q\mu}{eZ}\right)^2 \left(\frac{1}{2} \frac{q}{Mc} \frac{\mu/\mu_N}{Z}\right)^2, \quad (23)$$

where Z is the nuclear charge, μ the magnetic moment of the scatterer, μ_N the nuclear magneton, and M the nucleon mass. This ratio is small for large Z and small magnetic moments, which is the case of medium and heavy nuclei; however, it increases with the momentum transfer. For the case of the nucleons it has been feasible to use Eq. (22) and separate F_{ch} and F_{mag} with high accuracy.^{19,20} In other elements however conditions are not favorable; the slope of the straight line is small and the precision in its determination poor.

An obvious solution is to extend the measurements to such large angles that the increase in $\tan^2 \frac{1}{2}\theta$ compensates the smallness of $B(q)$. In particular, if one makes measurements at exactly $\theta=180^\circ$ one has from (22)

$$\left(\frac{d\sigma}{d\Omega}\right)_{180^\circ} = B(q) \left(\frac{Z\alpha}{2\epsilon}\right)^2 \frac{E}{E'}. \quad (24)$$

The cross section is then purely magnetic and although small can be measured without the usually dominating contribution from charge scattering.

¹⁹ See, for example, D. Aitken, R. Hofstadter, E. B. Hughes, T. Janssens, and M. R. Yearian, in *Proceedings of the 1962 International Conference on High Energy Physics* (CERN, Geneva, 1962), p. 185.

²⁰ The Mott cross section is really proportional to

$$[1 - (v/c)^2 \sin^2 \frac{1}{2}\theta],$$

which for $v \rightarrow c$ becomes $\cos^2 \theta/2$.

A special method is necessary to measure cross sections at 180°; the reason is that the detection of the scattered electrons is usually made in magnetic spectrometers which for structural reasons cannot swing to angles larger than ~150° without the incident beam of electrons hitting the spectrometer pole faces or mount. In the method developed at Stanford University by Peterson and Barber²¹ electrons are deflected ~10° by an auxiliary magnet before striking the target and the ones scattered at 180° are deflected again approximately 10° (in the opposite direction) before entering a magnetic spectrometer located at 160° with respect to the incident beam. A sketch of this experimental setup is given in Fig. 3. Other arrangements are possible and are in use at Stanford, Orsay, and other laboratories.

In general what one measures in magnetic scattering experiments is the complete spectrum of electrons scattered by a target at some large angle ($\theta \sim 180^\circ$) when

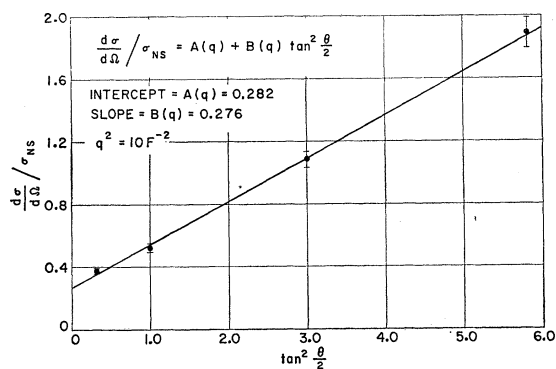


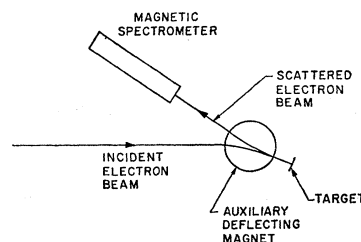
FIG. 2. Typical plot of the differential cross section for scattering as a function of $\tan^2 \frac{1}{2}\theta$. This corresponds to electron-proton scattering data at a $q^2 = 10 \text{ F}^{-2}$.

electrons of incident energy E_0 are incident upon it. Figure 4 shows a sketch of the expected features of this spectrum. This sketch shows six regions in the spectrum which we discuss separately:

1. In region "a" one has magnetic elastic scattering by the magnetic moment of the nucleus, as well as a contribution from electrons that are scattered by the charge of the nucleus but enter the detector for reasons discussed below.
2. In region "b" discrete nuclear energy levels are excited. It is shown later that they correspond mainly to magnetic multipole transitions; at low incident electron energies they constitute what one could call a "giant magnetic-dipole resonance."
3. In region "c" electric-dipole transitions resulting from the transverse terms in the electromagnetic interactions of the electrons are outstanding; they correspond to the "giant electric-dipole resonance," which is generally studied with real photons.

²¹ G. A. Peterson and W. C. Barber, *Phys. Rev.* **128**, 812 (1962).

FIG. 3. Sketch of the experimental arrangement for 180° scattering in use at the Mark II Stanford Accelerator.



4. Region "d" corresponds to quasielastic scattering, i.e., scattering of electrons by the many individual nucleons; the shape of this broad "peak" is determined by the momentum distribution of the nucleons inside the nucleus.

5. Region "e" corresponds to the high-energy tail of the momentum distribution where short-range correlations are expected to appear.

6. In region "f" electrons that have lost energy through radiation are dominant; these can be attributed to the basic process of bremsstrahlung at very large angles or to such processes as radiation by an electron that was already degraded in energy by a previous scattering. Electrons of this origin are present also in the other regions and are represented by the dotted line in Fig. 4. The "nuclear physics" features of the spectrum are therefore superimposed on a continuous spectrum of electrons that have a basically different origin. Furthermore the radiative corrections (Schwinger correction) contributes in an important way to this continuous spectrum. These contributions make up what is generally called the "radiation tail," which must be subtracted before any interpretation of the nuclear physics can be made.

Measurements of cross sections at 180° have special problems associated with them. The basic ones are:

- (a) The cross section at 180° is a minimum and it increases very rapidly because of the charge-scattering contributions (which goes as $\cos^2 \frac{1}{2}\theta / \sin^4 \frac{1}{2}\theta$) as the

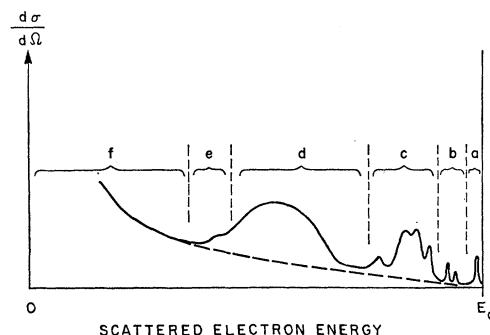


FIG. 4. Regions of the spectrum of high-energy electrons scattered at large angles by a nucleus: Region "a"—magnetic elastic scattering; region "b"—magnetic dipole transitions; region "c"—electric dipole transitions; region "d"—quasielastic scattering; region "e"—tail of quasielastic peak; region "f"—radiation tail. The dotted line represents the radiation tail in regions "b", "c", "d", and "e".

angle decreases from 180° ; on the other hand, spectrometers have a finite entrance angle (typically 0.01 sr) and consequently some charge scattering enters the spectrometer. A solution of this problem is to measure an angular distribution about 180° ; since the magnetic scattering is proportional to $1/\sin^4 \frac{1}{2}\theta$ and the charge scattering to $\cos^2 \frac{1}{2}\theta/\sin^4 \frac{1}{2}\theta$ these contributions can be separated.

(b) The multiple scattering of electrons in the target either before or after scattering can represent a considerable complication to the experiment since it effectively increases the entrance angle of the spectrometer in an energy dependent way; at low energies and for thick targets considerable care must be taken with this effect.

(c) The radiation tail at 180° cannot be calculated using the usual approximate formulas which deal only with bremsstrahlung by the nuclear charge. Not only a better expression for this spectrum has to be used but in addition the bremsstrahlung resulting from the magnetic moment of the nucleus (if it has one) has to be considered. This point is discussed in greater detail in Sec. III.

III. EXTRACTING INFORMATION ON NUCLEAR STRUCTURE

A. Bremsstrahlung at Large Angles

The spectrum of electrons scattered at a given angle, regardless of the direction of the accompanying photon in the bremsstrahlung process, has been calculated by Parzen *et al.*²² for point nuclei with no magnetic moment. We are interested here in finite-size nuclei with magnetic moments. Calculations have been made for this problem by Ginsberg and Pratt²³ in Born approximation, neglecting nuclear recoil and processes in which the nucleus is left in excited states.

The differential cross section for bremsstrahlung from a nucleus with a charge and magnetic moment, after summing over final electron and nuclear spins, photon polarizations, and averaging over initial electron and nuclear spins, was found to be

$$\frac{d\sigma}{d\Omega_p d\Omega_k} = \frac{\Phi}{(2\pi)^2} \frac{p'}{p} \frac{dk}{k} \frac{1}{\Delta^4} \times \left\{ |F_{\text{oh}}|^2 T_{\text{oh}} + \left(\frac{\mu}{Ze}\right)^2 \left(\frac{I+1}{3I}\right) \Delta^2 |F_{\text{mag}}|^2 T_{\text{mag}} \right\}, \quad (25)$$

with the notation:

$$\begin{aligned} \Phi &= Z^2 r_0^2 / 137, \\ \hbar &= c = m_e = 1, \\ \mathbf{p}, \epsilon &\text{ initial electron momentum and energy,} \\ \mathbf{p}', \epsilon' &\text{ scattered electron momentum and energy,} \\ \mathbf{k}, k &= \epsilon - \epsilon' \text{ photon momentum and energy,} \\ \Delta &= \mathbf{p} - \mathbf{p}' - \mathbf{k} \text{ 3-momentum transfer,} \\ I, \mu &= \lambda e / 2M_p \text{ nuclear spin and magnetic moment,} \\ M_p &\text{— nucleon mass.} \end{aligned}$$

T_{oh} is the familiar expression from the Bethe-Heitler equation and T_{mag} is a similar function of $\mathbf{p}, \mathbf{p}', \mathbf{k}, \epsilon,$ and ϵ' . The form factors F_{oh} and F_{mag} for the nuclear charge and magnetic-moment distributions are, respectively,

$$\begin{aligned} F_{\text{oh}}(\Delta) &= (Z\alpha)^{-1} \int \rho(\mathbf{r}) \exp(i\Delta \cdot \mathbf{r}) d\mathbf{r}, \\ F_{\text{mag}}(\Delta) &= i\mu^{-1} \int \mu(\mathbf{r}) \exp(i\Delta \cdot \mathbf{r}) d\mathbf{r}. \end{aligned} \quad (26)$$

These are exactly the same form factors that enter in the elastic scattering cross sections, as we see later.

The spectrum of the electrons that constitutes part of the radiation tail can be obtained from Eq. (25) by integrating over the photon angles $d\Omega_k$. The result is

$$\frac{d\sigma}{d\epsilon' d\Omega} = \frac{\Phi}{4\pi} \frac{p'}{p} \int_{\chi_{\text{min}}}^{\chi_{\text{max}}} \frac{d\chi}{\chi^2} \left\{ |F_{\text{oh}}|^2 R_{\text{oh}} + \left(\frac{\mu}{Ze}\right)^2 \left(\frac{I+1}{3I}\right) 2\chi |F_{\text{mag}}|^2 R_{\text{mag}} \right\}, \quad (27)$$

where

$$\begin{aligned} R_{\text{oh}} &= -2a^{-1} - (2\epsilon^2 - \chi)(\alpha\beta_0 + \chi\beta) X^{-\frac{1}{2}} - (2\epsilon'^2 - \chi)(\alpha\beta + \chi\beta_0) X_0^{-\frac{1}{2}} \\ &\quad + \{2(\epsilon^2 + \epsilon'^2) + \alpha - \chi - 2[(1+\alpha)(\epsilon^2 + \epsilon'^2 - \chi) - k^2](\alpha - \chi)^{-1}\} (X^{-\frac{1}{2}} - X_0^{-\frac{1}{2}}), \end{aligned} \quad (28)$$

$$\begin{aligned} R_{\text{mag}} &= 2a^{-1}(2p^2 + \chi)(\alpha\beta_0 + \chi\beta) X^{-\frac{1}{2}} - (2p'^2 + \chi)(\alpha\beta + \chi\beta_0) X_0^{-\frac{1}{2}} \\ &\quad + \{2(\epsilon^2 + \epsilon'^2) - \alpha + \chi - 2[(1+\alpha)(p^2 + p'^2 + \chi) - k^2](\alpha - \chi)^{-1}\} X^{-\frac{1}{2}} - X_0^{-\frac{1}{2}}, \end{aligned} \quad (29)$$

²² P. T. McCormick, D. G. Keiffer, and G. Parzen, Phys. Rev. **103**, 29 (1956).

²³ Edward S. Ginsberg and R. H. Pratt, Phys. Rev. **134**, B773 (1964); **137**, B1500 (1965).

and where

$$\begin{aligned}
 \mathbf{q} &= \mathbf{p} - \mathbf{p}', & a &= |\mathbf{q}|, \\
 \chi_{\min} &= \frac{1}{2}\Delta_{\min}^2 = \frac{1}{2}(a - k)^2, \\
 \chi_{\max} &= \frac{1}{2}\Delta_{\max}^2 = \frac{1}{2}(a + k)^2, \\
 \alpha &= \epsilon\epsilon' - \mathbf{p}' \cdot \mathbf{p} - 1, \\
 \beta_0 &= \mathbf{q} \cdot \mathbf{p} = p^2 - \mathbf{p} \cdot \mathbf{p}', \\
 \beta &= \mathbf{q} \cdot \mathbf{p}' = \mathbf{p} \cdot \mathbf{p}' - p'^2, \\
 X_0 &= p^2\chi^2 + 2\chi[k^2 - \alpha(\epsilon'\epsilon_0 - 1)] + p'^2\alpha^2, \\
 X &= p'^2\chi^2 + 2\chi[k^2 - \alpha(\epsilon'\epsilon - 1)] + p^2\alpha^2.
 \end{aligned} \tag{30}$$

Equation (27) is the exact Born-approximation result for the spectrum of scattered electrons due to bremsstrahlung from a static spherically symmetric distribution of charge and magnetic moment.

In the limit of point nuclei, high incident energies and large scattering angles one obtains

$$d\sigma = d\sigma_{\text{oh}} + d\sigma_{\text{mag}},$$

with

$$d\sigma_{\text{oh}} = \frac{\Phi}{2\pi} \frac{p'}{p} \frac{d\epsilon'}{k} \frac{d\Omega_{p'}}{\epsilon^2} [A_{\text{oh}}(\gamma, \theta) \log 2\epsilon + B_{\text{oh}}(\gamma, \theta)], \tag{31}$$

$$d\sigma_{\text{mag}} = \frac{\Phi}{2\pi} \frac{p'}{p} \frac{d\epsilon'}{k} d\Omega_{p'} \left(\frac{2\mu}{Ze}\right)^2 \left(\frac{I+1}{3I}\right) [A_{\text{mag}}(\gamma, \theta) \log 2\epsilon + B_{\text{mag}}(\gamma, \theta)], \tag{32}$$

and

$$\begin{aligned}
 A_{\text{oh}}(\gamma, \theta) &= \frac{(1+\gamma^2)^2 \cos^2 \frac{1}{2}\theta}{2\gamma^3 \sin^4 \frac{1}{2}\theta}, \\
 A_{\text{mag}}(\gamma, \theta) &= \frac{(1+\gamma^2)(1 + \sin^2 \frac{1}{2}\theta)}{\gamma \sin^2 \frac{1}{2}\theta}, \\
 B_{\text{oh}}(\gamma, \theta) &= \frac{1+\gamma^2}{2\gamma^3} \left\{ \frac{\cos^2 \frac{1}{2}\theta}{\sin^4 \frac{1}{2}\theta} \log \gamma - \frac{1+\gamma^2}{2 \sin^4 \frac{1}{2}\theta} + \frac{1-\gamma+\gamma^2}{\sin^2 \frac{1}{2}\theta} + \left(\frac{\gamma}{\sin^4 \frac{1}{2}\theta} - \frac{2\gamma^2}{(1+\gamma^2) \sin^2 \frac{1}{2}\theta} \right) \log(\sin^2 \frac{1}{2}\theta) \right\}, \\
 B_{\text{mag}}(\gamma, \theta) &= \frac{1-\gamma}{\gamma} \log \gamma - \frac{1 + \sin^2 \frac{1}{2}\theta}{\sin^2 \frac{1}{2}\theta} + \sigma \log \left(\frac{1+\sigma}{1-\sigma} \right) + \left(1 + \frac{1+\gamma^2}{2\gamma \sin^2 \frac{1}{2}\theta} \right) \log(\gamma \sin^2 \frac{1}{2}\theta).
 \end{aligned} \tag{33}$$

In these expressions, $\gamma = \epsilon'/\epsilon$ and

$$\sigma = (1-\gamma)[(1-\gamma)^2 + 4\gamma \sin^2 \frac{1}{2}\theta]^{-\frac{1}{2}}.$$

The result for $d\sigma_{\text{oh}}$ was obtained by Parzen *et al.*²² The structure of Eq. (31) is interesting since the term $A_{\text{oh}}(\gamma, \theta)$, which is dominant at all angles except near 180° , has the familiar $\cos^2 \frac{1}{2}\theta / \sin^4 \frac{1}{2}\theta$ and thus is important where the charge scattering cross section is. The approximate formulas used at forward angles consider only this first term. However, B_{oh} contains terms which do not vanish with $\cos^2 \frac{1}{2}\theta$ and so dominates the large-angle charge bremsstrahlung. [In Eqs. (31)–(33) the electron mass has been neglected in comparison to the energy. As usual it is due to this approximation that charge scattering vanishes at 180° ; the corrections due to finite m_e must in some circumstances be considered.]

The ratio of the magnetic to the charge elastic bremsstrahlung for the point case [Eq. (32) divided by Eq. (31)] is

$$\frac{d\sigma_{\text{mag}}}{d\sigma_{\text{oh}}} = \left(\frac{\lambda}{Z}\right)^2 \left(\frac{I+1}{3I}\right) \left(\frac{\epsilon}{M}\right)^2 \frac{A_{\text{mag}} \log 2\epsilon + B_{\text{mag}}}{A_{\text{oh}} \log 2\epsilon + B_{\text{oh}}}, \tag{34}$$

where we have put $\mu = \lambda e / 2M$. As expected, the magnetic bremsstrahlung is most appreciable at $\theta = 180^\circ$, where $A_{\text{oh}} = 0$, and becomes less important as Z increases. For fixed γ and θ as $E \rightarrow \infty$ the magnetic bremsstrahlung becomes relatively more and more important. In Fig. 5, we illustrate the relative contributions of the point charge and point magnetic moment for $E = 54$ MeV and $\theta = 180^\circ$ using Eqs. (3) and (4). The contribution of the magnetic bremsstrahlung is large for scattered electrons undergoing small energy

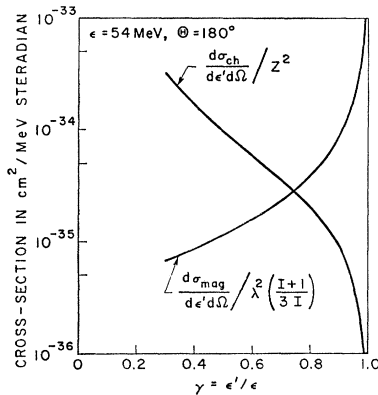


FIG. 5. Relative contributions to the radiative tail of the elastic peak from a point charge (Ze) and point magnetic moment ($\lambda e/2M_p$) in the limit $\epsilon, \epsilon' \gg 1, \theta \gg \epsilon^{-1}$.

loss, i.e., near the elastic peak from magnetic scattering. The relative importance of the magnetic bremsstrahlung can be inferred from Fig. 5 by multiplying the ratio of the two curves by the factor $(\lambda/Z)^2(I+1)/3I$, which in the case of Al^{27} is ≈ 0.037 yielding a ratio of $d\sigma_{mag}/d\sigma_{ch} \approx 0.026$ for $\gamma=0.7$ and ≈ 1.75 at $\gamma=0.95$. (For Cu these percentages are reduced by a factor of 10.)

Recently magnetic bremsstrahlung in electron-proton scattering has been observed for the first time. This constitutes an interesting problem in itself. Figure 6 shows the results of a measurement of the elastic peak in hydrogen for an incident energy of 54 MeV and a scattering angle of 180° .²⁴ The experimental points have not been corrected for magnetic bremsstrahlung. The dashed curve represents our approximate theoretical result for the elastic magnetic bremsstrahlung given by Eq. (32). (At these energies effects of the finite size of the proton are small.) We have interpreted γ as the fraction of the peak energy, i.e., we replace E_0 by the peak energy (the effects of recoil are about 10%). It is encouraging that Eq. (32) agrees fairly well with the data.²⁵

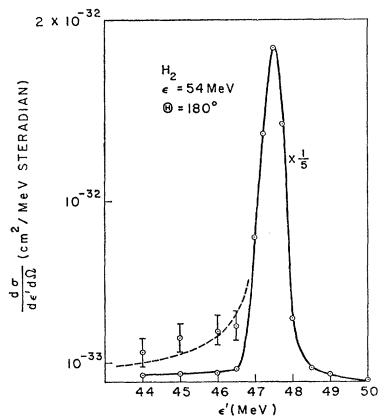


FIG. 6. Elastic peak in electron scattering from hydrogen (J. Goldemberg, unpublished). The dashed curve is the approximate analytic result for a point magnetic moment given by Eq. (32).

²⁴ J. Goldemberg (unpublished).

²⁵ Calculations for electron-proton bremsstrahlung that do not neglect proton recoil have been reported by R. A. Berg and C. N. Lindner, *Phys. Rev.* **112**, 2072 (1958); *Nucl. Phys.* **26**, 259 (1961). See also Y. Tsai, *Proceedings of the 1963 Conference on Nucleon Structure* (Stanford University Press, Stanford, 1964).

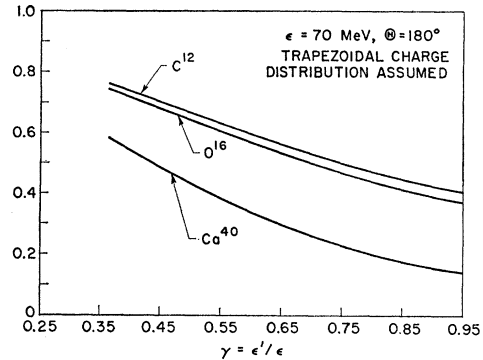


FIG. 7. Ratio of the cross section for scattered electrons after bremsstrahlung calculated with form factors (determined from elastic scattering) to the point charge result, for some spinless nuclei.

In the case of finite nuclei the integral in Eq. (27) can be evaluated numerically. The effect of finite nuclear extension in reducing the radiative tail is clearly shown in Fig. 7, where we have plotted the ratio of cross section, given by Eq. (27), to the point cross section, for some spinless nuclei (the situation is not complicated by the presence of magnetic bremsstrahlung). For simplicity, we have chosen a form factor corresponding to a trapezoidal charge distribution for all three nuclei, with values of the half radius and skin thickness taken from Table 3 of Herman and Hofstadter.²

Finally, in Fig. 8, we illustrate the effect of the contribution of magnetic bremsstrahlung. Inelastic scattering experiments have been performed on Li^7 at 180° using 41.5-MeV incident electrons.²⁶ This nucleus

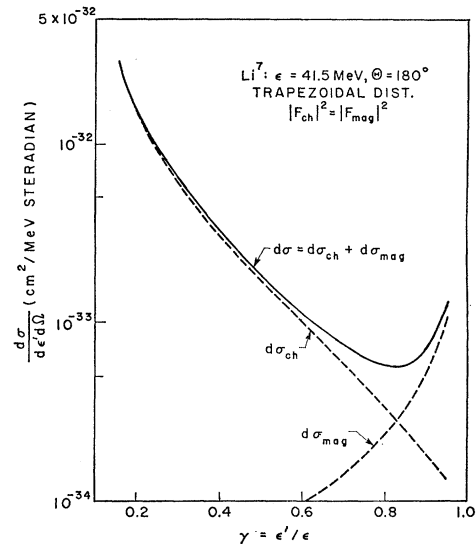


FIG. 8. Spectrum of scattered electrons due to bremsstrahlung from Li^7 , showing contribution of the charge and magnetic-moment distributions.

²⁶ W. C. Barber, J. Goldemberg, G. A. Peterson, and Y. Torizuka, *Nucl. Phys.* **41**, 461 (1963).

has a large magnetic moment and a low Z [the factor $(\lambda/Z)^2(I+1)/3I$ is approximately 0.65] so we expect magnetic effects to be important. As a first approximation we may set $|F_{\text{ch}}|^2 = |F_{\text{mag}}|^2$ and assume a trapezoidal form factor with parameters taken from Herman and Hofstadter.² Besides the differential cross section, the separate contributions of $d\sigma_{\text{ch}}$ and $d\sigma_{\text{mag}}$ are also shown in Fig. 6. The ratio $d\sigma_{\text{mag}}/d\sigma_{\text{ch}}$ is about 0.24 at $\gamma=0.7$ and rises up to 8.0 at $\gamma=0.95$. [This compares with ratios for the point case from Eq. (22) of 0.25 and 17.4, respectively.]

Maximon and Isabelle²⁷ have extended these calculations in order to include inelastic scattering; in their integration of the Bethe-Heitler formula they separate terms of order $\ln E/mc^2$ ("peak contribution") which are dominant at most angles and terms of order unity ("background contribution") which are in general neglected at forward angles,²⁸ but which become dominant at angles near 180° .

B. Radiative Corrections

These corrections are well known and have been used extensively in the literature; they account for the fact that in a scattering event there are higher order corrections (such as emission and absorption of virtual photons and emission of many low energy photons) which are responsible for the removal of electrons from a peak to a continuous spectrum that extends down to lower energies.

To obtain the real cross section of the peak it is then necessary to multiply the observed cross section by a correction factor. If one divides the spectrum of electrons in bins of width $\delta\epsilon$ starting at the highest energy at which electrons are present (ϵ') then the cross section in the highest energy bin is given by

$$(d\sigma/d\Omega)_{\text{real}} = (d\sigma/d\Omega)_{\text{observed}} \exp [y(\delta\epsilon)] \quad (35)$$

where y is given by Tsai²⁹ as

$$y(\delta\epsilon) = (2\alpha/\pi) \times \left\{ \left[\ln(\epsilon/\eta^2\delta\epsilon) + \frac{1}{2} \ln(\epsilon/\delta\epsilon) - \frac{1}{2} \right] [2m(q^2/M^2) - 1] + \frac{7}{8} \right\}, \quad (36)$$

where α is the fine-structure constant, M is the nucleon mass, and

$$\eta = 1 + (2\epsilon \sin^2 \frac{1}{2}\theta / Mc^2). \quad (37)$$

In the case of a spectrum of electrons such as the one in Fig. 4 in which one has not only an elastic peak but others as well, the radiative correction is applied using an iterative procedure that treats all the scattered electrons (elastic and inelastic) in a similar way³⁰: the

²⁷ L. C. Maximon and D. B. Isabelle, Phys. Rev. **133**, B1344 (1964); **136**, B674 (1964).

²⁸ L. I. Schiff, Phys. Rev. **87**, 750 (1952).

²⁹ Y. S. Tsai, Phys. Rev. **122**, 1898 (1961); see also N. T. Meister and D. R. Yennie, *ibid.* **130**, 1210 (1963), and N. T. Meister and T. A. Griffy, *ibid.* **133**, 1032 (1964).

³⁰ H. Crannell (private communication).

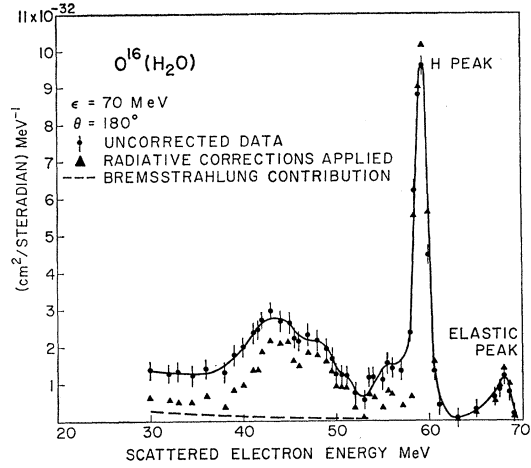


Fig. 9. Spectrum of electrons, initially 70 MeV, after scattering 180° from a water target. Shown also are the experimental points after the radiative correction (Schwinger correction) has been applied. The dotted line represents the bremsstrahlung contribution.

cross section of the second bin [between the energies $(\epsilon - 2\delta\epsilon)$ and $(\epsilon - \delta\epsilon)$] is reduced by the amount that comes from electrons that would have been at higher energies had there been no radiative corrections and then multiplied by its own e^y factor to correct for the electrons that were removed from it. A similar procedure is applied to the third bin and so on. This iterative procedure can be programmed in a computer and other corrections such as energy loss, electron-electron collisions, etc., incorporated. Alternatively the radiation tail can be computed using analytical expressions instead of being extracted by the procedure described above.³¹ These problems have also recently been discussed by Nguyen-Ngoc and Perez-y-Jorba.³²

As an example of the application of the methods discussed in this section, Fig. 9 shows the uncorrected data obtained from the scattering of 70-MeV electrons in a H_2O (water) target at a scattering angle of $\sim 180^\circ$, and the importance of the corrections.

IV. INTERPRETING INFORMATION ON NUCLEAR STRUCTURE

A. General Remarks³³

In agreement with our general result, the formula for the differential cross section for an unpolarized electron beam to scatter through an angle θ and at the same time take an unoriented nucleus from the state $J_i \rightarrow J_f$ is given in Born approximation (which should be good if Z is not too large), and with the neglect of nuclear

³¹ D. B. Isabelle and G. R. Bishop, Nucl. Phys. **45**, 209 (1963).

³² H. Nguyen-Ngoc and J. P. Perez-y-Jorba, Phys. Rev. **136**, B1036 (1964).

³³ R. H. Pratt, J. D. Walecka, and T. A. Griffy, Nucl. Phys. **64**, 677 (1965).

recoil, and the electron mass by³⁴⁻³⁶

$$\begin{aligned} & (d\sigma/d\Omega) (J_i \rightarrow J_f) \\ &= \frac{8\pi\alpha^2}{q^4} \left(\frac{p'k}{pk} \right) [V_L(\theta)W_L(q^2) + W_T(\theta)W_T(q^2)], \quad (38) \end{aligned}$$

where the nuclear structure form factors are

$$\begin{aligned} W_L(q^2) &= \sum_{L=0}^{\infty} (2J_i+1)^{-1} | (J_f || M_L(\Delta) || J_i) |^2, \\ W_T(q^2) &= \sum_{L=1}^{\infty} (2J_i+1)^{-1} \\ &\times \{ | (J_f || T_{J^{\text{mag}}}(\Delta) || J_i) |^2 + | (J_f || T_{J^{\text{el}}}(\Delta) || J_i) |^2 \}, \quad (39) \end{aligned}$$

with the following definitions³⁷:

$$\begin{aligned} V_L(\theta) &= (q^4/\Delta^4) 2p' p' \cos^2 \frac{1}{2}\theta \xrightarrow{p=p'} 2P^2 \cos^2 \frac{1}{2}\theta, \\ V_T(\theta) &= (2p' p'/\Delta^2) \sin^2 \frac{1}{2}\theta \\ &\times [(p+p')^2 - 2pp' \cos^2 \frac{1}{2}\theta] \xrightarrow{p=p'} p^2 (1 + \sin^2 \frac{1}{2}\theta), \quad (40) \end{aligned}$$

$\mathbf{p}(\mathbf{p}')$ = initial (final) electron wave numbers, $\Delta^2 = (\mathbf{p} - \mathbf{p}')^2$ is the 3-momentum transfer, $q^2 = \Delta^2 - (\mathbf{p} - \mathbf{p}')^2$ is the relativistic invariant 4-momentum transfer. $M_{LM}(\Delta)$ is the L th multipole moment of the nuclear charge density,

$$M_{LM}(\Delta) = \int d\mathbf{x} \rho_N(\mathbf{x}) Y_{LM}(\Omega_x) j_L(\Delta x), \quad (41)$$

and the operators T_{LM}^{mag} and T_{LM}^{el} are the transverse multipole operators

$$\begin{aligned} T_{LM}^{\text{el}}(\Delta) &= \Delta^{-1} \int d\mathbf{x} \{ \mathbf{j}_N(\mathbf{x}) \cdot [\nabla_{\Lambda} j_L(\Delta x) \mathbf{Y}_{LL}^M(\Omega_x)] \\ &\quad + \Delta^2 j_L(\Delta x) \mathbf{Y}_{LL}^M(\Omega_x) \cdot \mathbf{u}_N(\mathbf{x}) \}, \quad (42) \end{aligned}$$

$$\begin{aligned} T_{LM}^{\text{mag}}(\Delta) &= \int d\mathbf{x} \{ \mathbf{u}_N(\mathbf{x}) \cdot [\nabla_{\Lambda} j_L(\Delta x) \mathbf{Y}_{LL}^M(\Omega_x)] \\ &\quad + j_L(\Delta x) \mathbf{Y}_{LL}^M(\Omega_x) \cdot \mathbf{j}_N(\mathbf{x}) \}, \quad (43) \end{aligned}$$

³⁴ L. I. Schiff, Phys. Rev. **96**, 765 (1954).

³⁵ K. Alder, A. Bohr, T. Huus, B. Mottelson, and A. W. Winther, Rev. Mod. Phys. **28**, 476 (1956).

³⁶ The main effect of including nuclear recoil is to add a phase-space factor

$$[dW_f/dP_f]^{-1} = \{1 + [(P' - P \cos \theta)/E_f]\}^{-1},$$

where E_f is the final total energy of the target.

³⁷ The use of the 3-momentum transfer Δ in the form factors that appear in electron-scattering formulae indicates that the target is treated nonrelativistically (no recoil). For the case of elastic scattering in this approximation one has $q^2 = \Delta^2$. Since a relativistic generalization would probably contain the 4- instead of the 3-momentum transfer this substitution is made usually. For inelastic scattering in general $p \approx p'$, and consequently again $q^2 \approx \Delta^2$. In the case of excitation by real photons, on the other hand, $q^2 = 0$ and $\Delta = E_f - E_i$ (excitation energy).

where $\mathbf{j}_N(\mathbf{x})$ is the nuclear convection current density and $\mathbf{u}_N(\mathbf{x})$ is the spin magnetization density. The \mathbf{Y}_{LL}^M are the vector spherical harmonics as defined in Edmonds.³⁸ The transverse multiple operators are exactly the same as those governing radiative γ transitions in nuclei.³⁹ The only difference in the latter case is that there $|\Delta| = E_f - E_i$ (E_f and E_i are the initial and final energies of the nucleus) while here it is the momentum transferred by the electron.

We note the following important feature of the differential cross section. If we fix Δ , and then look in the backward direction, $\theta/2 = \pi/2$, only the *transverse multipole terms* contribute. If we further restrict to elastic scattering as in the experiments of Goldemberg and Torizuka,⁴⁰ then $J_f = J_i \equiv J$, and there is no parity change since the final and initial states are just the nuclear ground state. In this case the selection rules are

$$\begin{aligned} 1 \leq L \leq 2J \\ \Delta\pi = N0. \end{aligned}$$

This means we can have $M1$, $E2$, $M3$, $E4$, $M5$, $E6$ multipoles, etc. Time-reversal invariance eliminates the even electric multipoles.^{33,41} Thus only the odd magnetic transverse multipoles remain, $M1$, $M3$, $M5$, etc.

In the limit as the momentum transfer Δ goes to zero, we can make use of the fact that the transverse multipole operators are just those of γ decay, and use the results of Blatt and Weisskopf³⁹ for the ordering of the magnitude of the contributions of the various multipoles. [The expansion parameters are essentially $\Delta c/Mc^2$ and ΔR divided by the various factors that come into the expansions of the spherical Bessel functions $j_L(\Delta R)$.] The dominant multipole will be the $M1$. If we now use the fact that

$$\begin{aligned} T_{LM}^{\text{mag}}(\Delta) \xrightarrow{\Delta \rightarrow 0} \frac{iq\sqrt{2}}{3} \int d\mathbf{x} [\mathbf{u}_N(\mathbf{x}) + \frac{1}{2} \mathbf{x}_{\Lambda} \mathbf{j}_N(\mathbf{x})] \\ \cdot [\nabla \times Y_{1M}(\Omega_x)] = [iq/(6\pi)^{1/2}] \mu_{1M}, \quad (44) \end{aligned}$$

where μ_{1M} is just the magnetic-dipole operator, then we can relate the transverse $M1$ matrix element to the static magnetic moment by

$$(JJ | \mu_{10} | JJ) \equiv \mu$$

$$\begin{aligned} & (2J+1)^{-1} | (J || \mu_1 || J) |^2 \\ &= \left[\mu^2 \begin{pmatrix} J & 1 & J \\ -J & 0 & J \end{pmatrix}^{-2} \right] (2J+1)^{-1} (J+1) J^{-1} \mu^2. \quad (45) \end{aligned}$$

³⁸ A. R. Edmonds, *Angular Momentum in Quantum Mechanics* (Princeton University Press, Princeton, New Jersey, 1957).

³⁹ J. M. Blatt and V. F. Weisskopf, *Theoretical Nuclear Physics* (John Wiley & Sons, Inc., New York, 1952). This ordering does not remain valid for higher momentum transfers.

⁴⁰ J. Goldemberg and Y. Torizuka, Phys. Rev. **129**, 312 (1963).

⁴¹ L. Durand, P. DeCelles, and R. Marr, Phys. Rev. **126**, 1882 (1962).

Therefore,

$$\left. \frac{d\sigma}{d\Omega} \right|_{e_1} \xrightarrow{\Delta \rightarrow 0} \frac{8\pi\alpha^2 \left(\frac{k'}{k}\right)}{q^4} \left[V_L(\theta) \sum_{L=0}^{\infty} (2J+1)^{-1} |(J \| M_L(\Delta) \| J)|^2 + V_T(\theta) (2\pi)^{-1} \left(\frac{J+1}{3J}\right) \frac{\lambda^2 \hbar^2 \Delta^2}{4M^2 c^2} \right], \quad (46)$$

where $\mu \equiv \lambda \hbar / 2Mc$ (M is the nucleon mass). If we set $p' = p$ we find the simpler form³³

$$\left. \frac{d\sigma}{d\Omega} \right|_{e_1} \xrightarrow{\Delta \rightarrow 0} \left[\frac{\alpha^2 \cos^2 \frac{1}{2}\theta}{4k^2 \sin^4 \frac{1}{2}\theta} \right] \left[|F_{\text{oh}}(\Delta)|^2 + \left(\frac{J+1}{3J}\right) \left(\frac{\hbar^2 \Delta^2}{4M^2 c^2}\right) \lambda^2 (1 + 2 \tan^2 \frac{1}{2}\theta) \right], \quad (47)$$

where

$$|F_{\text{oh}}(\Delta)|^2 = \frac{4\pi}{2J+1} \sum_{L=0}^{\infty} |(J \| M_L(\Delta) \| J)|^2. \quad (48)$$

In the backward direction, as $\Delta \rightarrow 0$, one sees just the *static magnetic moment*. The above formula (if one sets $|F_{\text{oh}}(\Delta)|^2 = Z^2$) is identical with the formula originally derived by Jauch⁴² and independently by Scofield⁴³ for the scattering of an electron by a point system with a charge Z and magnetic moment λ .⁴⁴ The present derivation has the advantage that it holds for an extended target with arbitrary charge and current distribution and with any spin.

B. Elastic Scattering

As seen in the discussion above the magnetic scattering cross section given by Eq. (47) has a very simple structure that can be compared with experiment by measuring the scattering cross section at 180° as a function of Z at a given (small) momentum transfer. The form factors simplify in this case to $F_{\text{oh}} = Z^2$ and

$F_{\text{mag}} = \lambda$ and we get

$$\frac{1}{Z^2} \frac{d\sigma}{d\Omega} = \sigma_{\text{Mott}}^p \left\{ 1 + \frac{J+1}{3J} \frac{K^2}{Z^2} \frac{\hbar^2 \Delta^2}{4m^2 c^2} (1 + 2 \tan^2 \frac{1}{2}\theta) \right\}$$

$$\sigma_{\text{Mott}}^p = \left(\frac{e^2}{2\epsilon_0} \right)^2 \frac{\cos^2 \frac{1}{2}\theta}{\sin^4 \frac{1}{2}\theta}; \quad K = \mu / (e\hbar/mc). \quad (49)$$

At 180° there should not be any charge scattering but the finite solid angle of the spectrometer and scattering in the target (which is particularly important at low energies) gives an appreciable contribution to the cross section; the proper subtraction of this background constitutes an important part of this type of experiment (at low momentum transfers).

Figure 10 shows the data obtained for a number of elements by Goldemberg and Torizuka⁴⁰ using incident electrons of 41.5 MeV. The data are presented as the cross section divided by Z^2 . For spin-zero nuclei, $K=0$, and the cross section reduces to

$$(1/Z^2) (d\sigma/d\Omega) = \sigma_{\text{Mott}}^p = \text{constant}. \quad (50)$$

This is then a base line above which the magnetic scattering contribution appears. The solid line of Fig. 10 was obtained using Eq. (49) and the known static magnetic moments. Except for a few anomalies (B^{10} and B^{11}) agreement between theory and experiment is reasonable and one of the main features of the problem becomes clear: since the magnetic moment is attributable always (according to the shell model) to one or a few unpaired nucleons, it does not change much as Z increases; the Mott cross section however increases with Z^2 and thus the relative contribution of magnetic scattering decreases.

There are two ways in which the magnetic scattering can differ from that determined by the static limit of the magnetic moment, Eq. (49):

(i) The magnetic moment can have a structure and hence a form factor for elastic scattering. This is contained in the Δ dependence of $|(J \| T_1^{\text{mag}}(\Delta) \| J)|^2$. In particular, if the system has $J \leq 1$, and if Born

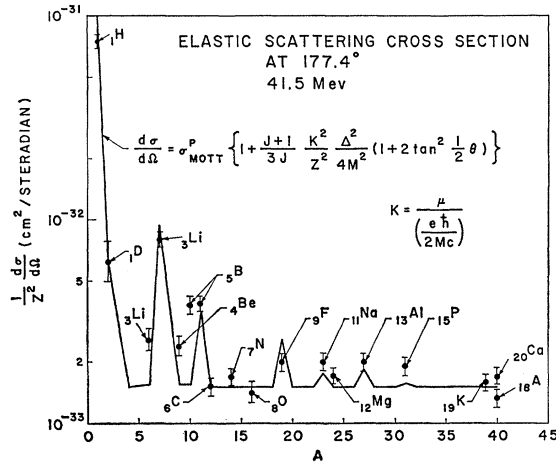


FIG. 10. The elastic magnetic cross section at 180° for light elements.

⁴² J. M. Jauch, *Helv. Phys. Acta* **13**, 451 (1940).

⁴³ J. Scofield (private communication).

⁴⁴ A similar result was obtained by R. Gatto, *Nuovo Cimento* **12**, 613 (1954), in a calculation of the scattering of muons by nuclei.

approximation is valid, this is *the only way* the scattering can differ.

(ii) The cross section will always be *increased* by the contributions of the higher multipoles which can contribute. Thus one might expect that the higher the spin J , the faster one will see a *positive* deviation from the cross section containing just the static moment. This is probably the case for B^{10} , which has an anomalously large magnetic scattering cross section.

The two effects above tend to compensate each other if the magnetic-moment form factor is a decreasing function of Δ as is usually true (but does not *have* to be true). The second effect is only seen for $J \geq \frac{3}{2}$.

In order to learn about the spatial distribution of the magnetic moment one has to make measurements at a variety of momentum transfers. In the shell model the orbits are expected to be fairly well defined in space and consequently pronounced maxima and minima might be expected in the differential cross section for magnetic scattering; while the charge scattering probes the nuclear charge as a whole, magnetic scattering probes in general the part of the nucleus responsible for the nuclear magnetic moment.

Furthermore exchange currents contribute to the magnetic scattering although they do not contribute to charge scattering. As is well known, electric multipole moment operators are independent of exchange effects⁴⁵ (Siegert's theorem)⁴⁶; the reason is that the electric multipoles depend on the charge distribution only while the magnetic moments are determined by both the charge and current distribution. In other words, in making predictions concerning electric moments or electric-multipole transitions one can feel reasonably secure even if one does not have a full knowledge of the exchange effects. However, the wavefunctions are needed (and might be affected by the exchange currents) but in general either they are known by other methods (as in the deuteron) or can be calculated according to some model. The study of electric multipoles constitutes then a test of how good they are.

In the study of magnetic-multipole transitions or moments one can only test the adequacy of the wave functions if all the exchange contributions are known at the outset. Consequently, if one knows the wave function (as in the case of the deuteron), one can obtain information on the exchange contributions.

Somewhat detailed studies of elastic magnetic scattering have been made for the deuteron, tritium and helium-3 and helium-4; we discuss them briefly. Very few measurements have been made of the form factors of nuclei heavier than He^4 . Results have recently been

reported for Li^6 , Li^7 , Be^9 , B^{10} , B^{11} , and N^{14} ;⁴⁷ magnetic octupole moment effects have been observed. As an example of the form factor one can expect from a typical shell-model magnetic-moment distribution we give also in this section the calculation of the form factor for the magnetic scattering of F^{19} . Further shell-model calculations have been made by Griffy and Yu.⁴⁸

1. The Deuteron

The magnetic elastic-scattering cross section of the deuteron was measured at 180° at low momentum transfers (0.26 and 0.41 inverse fermis) by Goldemberg and Schaerf.⁴⁹ The measurements were made relative to the photon cross section. From the data, the magnetic moment of the deuteron at the q values mentioned above can be obtained (Fig. 11). Also available in the literature is the static magnetic moment of the deuteron which is known very precisely ($\mu_D = 0.857$ nm).

In the impulse approximation and neglecting exchange effects a simple nonrelativistic expression can be written for the static moment of the deuteron

$$\mu_D = \mu_S - \frac{3}{2}(\mu_S - \frac{1}{2})P_D, \quad (51)$$

where $\mu_S = \mu_P + \mu_N$; μ_P and μ_N are the static magnetic moments of the proton and neutron, respectively, and P_D is the D state probability in the deuteron ground state. This equation has been used in the past to determine P_D which comes out to be $\cong 0.04$.

Using the latest information on P_D obtained by analysis of the quadrupole moment of the deuteron,⁵⁰ of the photodesintegration studies⁵¹ and the coherent photoproduction of pions⁵² one obtains however $P_D \cong 0.07$. Using this value in Eq. (51) above one obtains $\mu_D = 0.84$. This is a well-known discrepancy in the value of the static value of the magnetic moment of the deuteron for which several explanations have been offered⁵³ (such as relativistic corrections, and exchange effects).

Measurements of the magnetic elastic scattering from the deuteron yield the magnetic moment as a function of the momentum transfer and therefore offer two

⁴⁷ R. E. Rand, R. Frosch, and M. R. Yearian, Phys. Rev. Letters **14**, 234 (1965); also Phys. Rev. (to be published); J. Goldemberg, D. B. Isabelle, T. Stovall, D. Vinciguerra, and A. Bottino, Phys. Letters **16**, 141 (1965); G. J. Vanpraet and P. Kussanyi-Demay, Nuovo Cimento **39**, 388 (1965). Early work is due to G. A. Peterson, Phys. Letters **2**, 162 (1962); and Goldemberg and Torizuka, Ref. 40.

⁴⁸ T. A. Griffy and D. U. L. Yu, Phys. Rev. **139**, B880 (1965).

⁴⁹ J. Goldemberg and C. Schaerf, Phys. Rev. Letters **12**, 298 (1964).

⁵⁰ R. Wilson, *The Nucleon-Nucleon Interaction* (Interscience Publishers, Inc., New York, 1963).

⁵¹ M. L. Rustgi, W. Zernik, G. Breit, and D. L. Andrews, Phys. Rev. **120**, 1881 (1960); M. Matsumoto, *ibid.* **129**, 1334 (1963); F. Partovi, Ann. Phys. (N.Y.) **27**, 79 (1964).

⁵² F. T. Hadjioannou, Phys. Rev. **125**, 1414 (1962); J. I. Friedman and H. W. Kendall, *ibid.* **129**, 2802 (1963); E. Erickson and C. Schaerf, Phys. Rev. Letters **11**, 432 (1963).

⁵³ G. Breit and R. M. Thaler, Phys. Rev. **89**, 1177 (1953).

⁴⁵ R. G. Sachs, *Nuclear Theory* (Addison-Wesley Publishing Co., Inc., New York, 1953), mainly pp. 241-258.

⁴⁶ The conditions for the validity of Siegert's theorem in electron scattering have been investigated recently by J. M. Eisenberg and M. E. Rose, Phys. Rev. **131**, 848 (1963).

additional pieces of information:

(a) An independent check on the absolute value of the magnetic moment of the deuteron can be obtained by extrapolation of the measurements to low momentum transfers. This is the information which may be obtained from the Goldemberg-Schaerf experiment, and as can be seen in Fig. 11 corroborates what is known for the static value of μ_D .

(b) The q dependence of the form factor can be calculated from theory and compared with experiments. Calculations were made using Gourdin's⁵⁴ formulae and the wave functions given by Breit *et al.*⁵¹ and $P_D=0.07$ (Fig. 11). The experiments described in Ref. 49 cover a rather limited region of momentum transfers to be very useful for this kind of comparison.⁵⁵

Calculations have been made recently by Harrington⁵⁶ and by Adler and Drell⁵⁷ on the contribution of 3-meson exchanges to the magnetic moment of the deuteron and the results are of the order of magnitude necessary to explain the experimental results.⁵⁸

The relativistic corrections to the magnetic moment of the deuteron have not been calculated yet in detail.

2. Tritium and Helium-3

After the deuteron, the simplest nuclear systems are the three-body mirror-nuclei H^3 (3 protons) and He^3 (2 protons, 1 neutron). Naively, one can think of these systems as formed by a pair of protons with spins up and down, thereby canceling their magnetic moments,

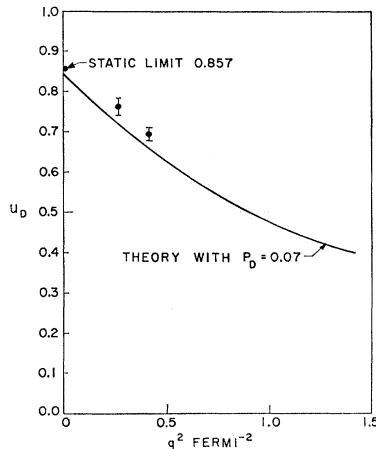


FIG. 11. The deuteron magnetic moment as function of the momentum transfer. The theoretical curve has been calculated with a D -wave contribution of 0.07.

⁵⁴ M. Gourdin, *Nuovo Cimento* **28**, 533 (1963).
⁵⁵ This experiment was extended to higher momentum transfers (up to $q^2=5$) recently by D. Drickey, D. Frerejacque, and D. Benaksas, *Phys. Rev. Letters* **13**, 353 (1964), and the q -dependence of the form factor effectively agrees with the theoretical predictions of the impulse approximation with no relativistic or exchange effects (Jankus formula).
⁵⁶ D. R. Harrington, *Phys. Rev.* **133**, B142 (1964).
⁵⁷ R. Adler and S. D. Drell, *Phys. Rev. Letters* **13**, 349 (1964).
⁵⁸ See also, D. J. Drickey and L. N. Hand, *Phys. Rev. Letters* **9**, 521 (1962).

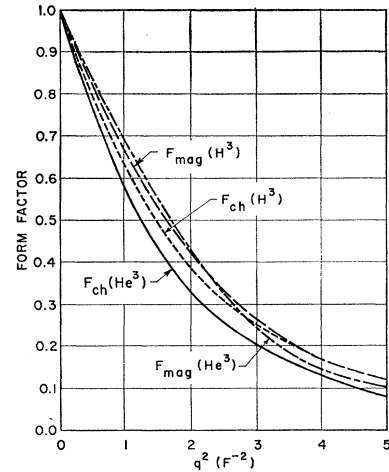


FIG. 12. H^3 and He^3 form factors as a function of momentum transfer.

so that the magnetic properties of the systems are then determined by the remaining nucleon (proton in H^3 and neutron in He^3). A detailed analysis of the magnetic moments of these nuclei in the light of the mirror theorem for nuclear moments⁴⁶ gives a clear indication of the existence of exchange currents in He^3 .

These nuclei have been recently investigated by electron scattering (both charge and magnetic) by Hofstadter and collaborators⁵⁹; the form factors obtained are shown in Fig. 12 where it is seen that they are approximately equal except for F_{ch} of He^3 which is appreciably larger than the others. The rms radius (R) that can be obtained are the following:

$$\begin{aligned} R_{ch}(H^3) &= 1.64 F & R_{mag}(H^3) &= 1.64 F \\ R_{ch}(He^3) &= 1.80 F & R_{mag}(He^3) &= 1.64 F. \end{aligned}$$

Thus there is a concentration of the magnetism of He^3 as compared to its charge distribution.

Schiff *et al.*⁶⁰ have made a detailed analysis of the data of Hofstadter *et al.* and derived among other things the form factor for the exchange part of the magnetic moment of He^3 .

3. Helium-4

Since He^4 has spin 0 and no static magnetic moment, Eq. (47) predicts that no magnetic scattering should be observed in this case. However the presence of a nonvanishing electric-dipole moment (edm) or "anomalous" magnetic moment for the electron (not the anomalous magnetic moment which has origin in electromagnetic corrections and can be shown to be unimportant at the momentum transfers at which the scattering experiments are performed⁶¹) would lead to

⁵⁹ H. Collard, R. Hofstadter, A. Johansson, R. Parks, M. Rynewel, A. Walker, M. R. Yearian, R. B. Day, and R. T. Wagner, *Phys. Rev. Letters* **11**, 387 (1963).
⁶⁰ L. I. Schiff, H. Collard, R. Hofstadter, A. Johansson, and M. R. Yearian, *Phys. Rev. Letters* **11**, 387 (1963).
⁶¹ S. D. Drell and F. Zachariasen, *Phys. Rev.* **111**, 1727 (1958).

a differential cross section given by⁶²

$$d\sigma/d\Omega = \sigma_M |F_{\text{oh}}(q)|^2 [1 + \alpha^2(q) (\hbar q/m_0c)^2 (\cos^2 \theta)^{-1}],$$

$$\alpha^2(q) = \lambda^2(q) + \mu^2(q), \tag{52}$$

where $\lambda(q)$ and $\mu(q)$ are the form factors of the edm or anomalous magnetic moment of the electron.

The second term inside the bracket is generally very small but becomes more important as q increases and also as $\theta \rightarrow 180$. Consequently one can measure $d\sigma/d\Omega$ at large angles and find out what is the value of $\alpha(q)$ necessary to explain the observed value. Bureson and Kendall⁶³ have done the experiment at angles up to 135° and have found that α in units of $e\hbar/m_0c$ was $< 2 \times 10^{-4}$.

Goldemberg and Torizuka⁶⁴ repeated the experiment at $\sim 180^\circ$ with the result that $\alpha \leq 3 \times 10^{-5} e\hbar/m_0c$. The experiment does not distinguish between an electric-dipole moment and an anomalous magnetic moment. Attributing the upper limit above to an edm one can say that the dipole moment of the electron is smaller than 10^{-15} e-cm. The limit placed on the same number by other methods such as an analysis of the Lamb-shift experiments are ~ 3 times larger. Rand⁶⁵ subsequently used 180° scattering from C^{12} at higher momentum transfers and obtained $\alpha \lesssim 6 \times 10^{-6} e\hbar/m_0c$.

4. Fluorine-19

As an example of the calculation of the form factors to be expected for large nuclei we reproduce here the calculation³³ of the magnetic elastic scattering form factor for F^{19} . We assign F^{19} as an odd proton in the $s_{1/2}$ state; since the known magnetic moment $\mu_F = +2.629$ agrees so well with the Schmidt value $\mu(\text{Schmidt}) = 2.79$, the single-particle shell model may be applied with some confidence. We have

$$T_{1M}^{\text{mag}}(\Delta) = \int d\mathbf{x} j_1(\Delta x) \mathbf{Y}_{111}^M(\Omega_x) \cdot [\mathbf{j}_N(\mathbf{x}) + \nabla_{\Lambda} \mathbf{u}_N(\mathbf{x})], \tag{53}$$

and we want to calculate $[(0\frac{1}{2})\frac{1}{2} || T_1^{\text{mag}}(\Delta) || (0\frac{1}{2})\frac{1}{2}]$ where the notation is $| (ls)j \rangle$. The first term can be written (for a single particle)

$$(i/\sqrt{2}) [\nabla j_1(\Delta x_i) Y_{111}^M(\Omega_{x_i})] \cdot \mathbf{l}_i \tag{54}$$

and since $\mathbf{l} | (0\frac{1}{2})\frac{1}{2} \rangle = 0$ this term makes no contribution. The second term can be written

$$\int d\mathbf{x} \mathbf{u}_N(\mathbf{x}) \cdot [\nabla_{\Lambda} j_1(\Delta x) \mathbf{Y}_{111}^M(\Omega_x)], \tag{55}$$

where $\mathbf{u}_N(\mathbf{x}) = \lambda_{\mu_0} \delta_i \delta(\mathbf{x} - \mathbf{x}_j)$ (for a single particle). With the aid of identities on the vector spherical harmonics in Edmonds³³ and using the fact that only the

⁶² B. Margolis, S. Rosendorff, and A. Sirlin, Phys. Rev. **114**, 1530 (1959).

⁶³ G. R. Bureson and H. W. Kendall, Nucl. Phys. **19**, 68 (1960).

⁶⁴ J. Goldemberg and Y. Torizuka, Phys. Rev. **129**, 2580 (1963).

⁶⁵ R. E. Rand, Phys. Rev. **140**, B1605 (1965).

$l=0$ part of the operator contributes, we find

$$T_{1M}^{\text{mag}}(\Delta) \rightarrow i\lambda \Delta \mu_0 (\frac{2}{3})^{\frac{1}{2}} j_0(\Delta x_i) [\delta_i \cdot \mathbf{Y}_{101}^M(\Omega_{x_i})]. \tag{56}$$

The only difference from the static case is the radial function $j_0(\Delta x)$. We can thus compute the form factor for the transition as

$$F(\Delta) = (N_{2s}/\sqrt{\pi}) \int |u_2^s(x)|^2 x^2 dx j_0(\bar{\Delta}x), \tag{57}$$

in the notation of Elliott and Lane⁶⁶ and the oscillator wave functions are

$$u_{2s}(x) = (x^2 - \frac{3}{2}) \exp(-\frac{1}{2}x^2),$$

$$N_{2s} = \frac{8}{3},$$

$$\bar{\Delta} \equiv \Delta \left(\frac{\hbar}{MW_{\text{osc}}} \right)^{\frac{1}{2}} = \left(\frac{\hbar^2 \Delta^2}{M} / \hbar W_{\text{osc}} \right)^{\frac{1}{2}}. \tag{58}$$

Computation of the integral gives

$$F(\Delta) = [1 - \frac{1}{3}\bar{\Delta}^2 + \frac{1}{24}\bar{\Delta}^4] \exp(-\frac{1}{4}\bar{\Delta}^2). \tag{59}$$

C. Inelastic Scattering in Levels

As one measures the energy spectrum of scattered electrons down from the elastic peak (region "b" of Fig. 4) some outstanding levels such as the one at 3.56 MeV in Li^6 are seen²⁶ (Fig. 13). This is a well-known 0^+ state and since the ground state of Li^6 is a 1^+ state, its excitation involves a magnetic-dipole transition. The same is the case for other levels of light nuclei such as the 15.1-MeV 1^+ level in C^{12} ; these are in general bound levels of nuclei and therefore quite narrow.⁶⁷ The presence of these levels is to be expected as one can see in Eq. (39) above; the transverse magnetic matrix elements are proportional to $(1 + \sin^2 \frac{1}{2}\theta)$ which has a maximum at 180° while the longitudinal matrix elements which are dominant at forward angles are proportional to $\cos^2 \frac{1}{2}\theta$ and vanish at 180° . However there is also present at 180° a transverse electric term which has the

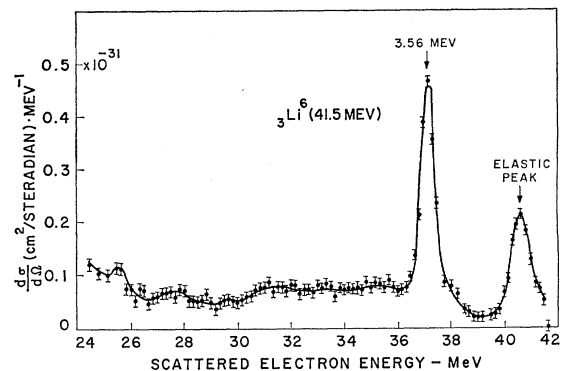


FIG. 13. Spectrum of 41.5-MeV electrons scattered from Li^6 at 180° .

⁶⁶ J. P. Elliot and A. M. Lane, in *Handbuch der Physik*, edited by S. Flügge (Springer-Verlag, Berlin, 1957), Vol. 39, p. 248.

⁶⁷ Further experiments on Na^{23} have recently been reported by W. C. Barber and G. J. Vanpraet, Nucl. Phys. **72**, 63 (1965).

same angular dependence as the magnetic transitions; distinction between them has to be made from independent information on their spins. In the limit of low momentum transfers the ordering of the different terms of the multipole expansion is the same as the one used in photon excitation so the dominant multipoles are electric dipole ($E1$) and magnetic dipole ($M1$).

The identification of transitions as $E1$ or $M1$ is not easy because they have the same angular distribution; information from other sources helps to establish their character but whenever this is not available the comparison of the q dependence of the form factor with models helps in making the distinction.

In comparing the measured cross sections with calculated matrix elements there is one important piece of information which can be included. That is the cross section for photoabsorption in the level considered. In this case the operators $T_{J^{\text{el}}}$ and $T_{J^{\text{mag}}}$ are *exactly* the same ones that describe emission and absorption of real photons but the relation between the momentum transfer and the energy of the photon is

$$E_f - E_i = E_{\text{excit}} = |\Delta_{\text{ph}}|. \quad (60)$$

Lewis and Walecka⁶⁸ have shown that the integrated absorption cross section in one level is given by

$$\int_{\text{level}} \sigma(\epsilon) d\epsilon = (2\pi)^3 \alpha E_{\text{excit}}^{-1} (J+1)^{-1} \times \sum \{ \langle J_f || T_{J^{\text{el}}}(\Delta_{\text{ph}}) || J_i \rangle^2 + \langle J_f || T_{J^{\text{mag}}}(\Delta_{\text{ph}}) || J_i \rangle^2 \} \quad (61)$$

In general, the parity of the transition allows only one of the matrix elements to contribute.

1. $M1$ Levels

These are the most outstanding levels in experiments at large angles because of the tendency for all the transition strength of $M1$ transitions to be concentrated in a few, generally one or two, levels. Furthermore, as bound levels their width is generally very small; this was predicted by shell-model calculations by Kurath⁶⁹ in $1p$ and $2s-1d$ shells and confirmed by experiments. The most outstanding levels are found in Be^9 , Li^6 , C^{12} , Mg^{24} , and Si^{28} .

Measurements were made recently on some of these levels for a number of momentum transfers.⁷⁰ We discuss only the 15.1-MeV level of C^{12} for which many experiments exist⁷¹ (Fig. 14).⁷² If one assumes the 15.1-MeV

⁶⁸ F. H. Lewis and J. D. Walecka, *Phys. Rev.* **133**, 849 (1964).

⁶⁹ D. Kurath, *Phys. Rev.* **130**, 1525 (1963).

⁷⁰ J. Goldberg, W. C. Barber, F. H. Lewis, and J. D. Walecka, *Phys. Rev.* **134**, B1022 (1964).

⁷¹ F. Gudden, *Phys. Letters* **10**, 313 (1964); B. Dudelzak and R. E. Taylor, *J. Phys. Radium* **22**, 544 (1961); H. Schmid and W. Scholz, *Z. Physik* **175**, 430 (1963).

⁷² In analyzing data of this kind one usually plots reduced transition probabilities B_{M1} which are related to the reduced matrix elements that appear in the formulae of this paper by the relation

$$(xc\Delta)^2 B_{M1}(1 \rightarrow 0, \Delta) = 5.28 \times 10^6 \langle 1 || T^{\text{mag}}(\Delta) || 0 \rangle^2.$$

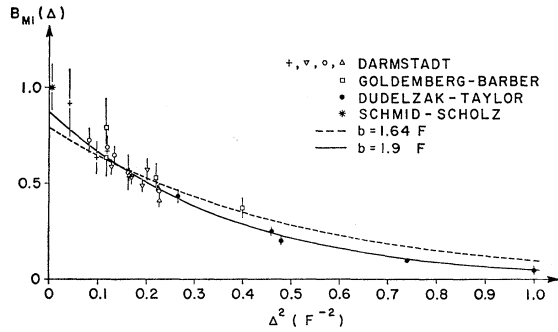


FIG. 14. The reduced transition probability $B_{M1}(1 \rightarrow 0)$ for the 15.1-MeV level in C^{12} as a function of the momentum transfer. The curves are calculated for different values of the harmonic oscillator parameter. The data are from various experiments.

level is due to single-particle transitions from the $(1p_{3/2})$ to the $(1p_{1/2})$ shell, and uses $j-j$ coupling,⁷⁰ one obtains for the reduced matrix element

$$\langle (1p_{3/2}) (1p_{1/2})^{-1}, J^\pi = 1^+, T = 0 | T_1^{\text{mag}}(\Delta) | J = 0, T = 0 \rangle^2 = (9\pi)^{-1} (g/M)^2 \{ [(\mu_P - \mu_N) - \frac{1}{2}] F_0^2(\Delta) + [\frac{1}{4}(\mu_P - \mu_N) - \frac{1}{2}] F_2^2(\Delta) \}, \quad (62)$$

where M is the proton mass, μ_P and μ_N the proton and neutron magnetic moments, and

$$F_l(\Delta) = \int_0^\infty [R_{1p}(r)]^2 j_l(\Delta r) r^2 dr, \quad (63)$$

where R_{1p} is the radial wave function for a particle in the $1p$ shell. Calculation of $F_0(\Delta)$ and $F_2(\Delta)$ using harmonic oscillator wave functions gives

$$F_0(\Delta) = \exp(-\frac{1}{4}x^2) [1 - \frac{1}{6}x^2], \quad (64)$$

$$F_2(\Delta) = \exp(-\frac{1}{4}x^2) [\frac{1}{6}x^2], \quad (65)$$

where $x = \Delta b$, b being the oscillator length parameter.

As seen in Eq. (62) the Δ dependence of the reduced matrix element is all contained in $F_0(\Delta)$ and $F_2(\Delta)$. Its absolute value depends on a coefficient related to the magnetic moments of the nucleons. It turns out that the absolute value depends sensitively on the assumed amount of spin-orbit coupling; however this choice has little effect on the radial dependence.⁷³ Two independent pieces of information can be obtained from experiments. The curves of Fig. 14 were drawn for a spin-orbit coupling ratio of $a/K = 4.6$ and two oscillator strengths; the best fit is obtained with an oscillator parameter $b = 1.9$ F, which is larger than the one obtained in the analysis of charge scattering experiments⁷⁴ ($b = 1.64$ F).

Calculations and measurements for other transitions were also made by Bishop.⁷⁵

⁷³ D. Kurath, *Phys. Rev.* **134**, B1025 (1964).

⁷⁴ U. Meyer-Berkhout, K. W. Ford, and A. E. S. Green, *Ann. Phys. (N.Y.)* **8**, 119 (1959).

⁷⁵ G. R. Bishop, *Phys. Letters* **8**, 128 (1964).

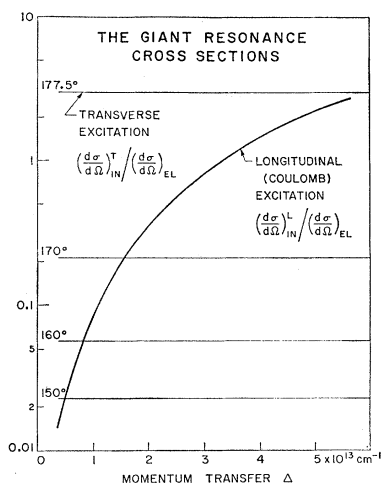


FIG. 15. The ratio of the transverse and longitudinal cross section to the elastic cross section as a function of the momentum transfer. For the transverse part this ratio is plotted for several angles of scattering.

2. $E1$ Levels

Electric-dipole transitions of low energy (≤ 10 MeV) are strongly suppressed in nuclei due to the existence of correlations between the neutrons and protons.⁷⁶ This can be understood simply by considering a system consisting of protons only; in such a system the electric center is the same as the center of mass; for every charge moving to the left there is an equal one moving to the right since the center of mass stays at rest; hence the dipole moment is always zero. In fact few electric-dipole transitions of low energy are known to exist. For higher excitation energies, however, more complicated motions of the neutrons and protons are possible⁷⁶ (such as moving all the neutrons against all the protons) and a strong electric-dipole transition may occur. These have been studied extensively by photon excitation, although experimental difficulties have prevented measurements of the detailed shape and absolute magnitude of most cross sections. The general name of "giant dipole resonance" is given to the group of levels (or continuum) in which strong electric-dipole absorption is observed; these occur in general between energies of 15 and 25 MeV and are not bound, so their widths are expected to be large enough to cause overlapping.

Inspection of Eq. (39) shows that these transitions can be investigated by inelastic electron scattering either at forward angles (through the longitudinal operators) or at large angles where only the transverse operators are present. An analysis of the most favorable conditions for the observation of the $E1$ "giant resonance" in electron scattering was made by Goldemberg *et al.*⁷⁷ using a simple model for the nucleus: protons oscillating as a unit against the neutrons—this is referred to sometimes as the Goldhaber-Teller model.⁷⁶

⁷⁶ M. Goldhaber and E. Teller, Phys. Rev. **74**, 1046 (1948).
⁷⁷ J. Goldemberg, Y. Torizuka, W. C. Barber, and J. D. Walecka, Nucl. Phys. **43**, 242 (1963).

In this model one obtains

$$\left(\frac{d\sigma}{d\Omega}\right)_{in}^L / \left(\frac{d\sigma}{d\Omega}\right)_{el} = \left(\frac{N}{A}\right)^2 \left(\frac{\Delta^2}{2\mu}\right) \omega^{-1} \quad (66)$$

for the longitudinal part,

$$\left(\frac{d\sigma}{d\Omega}\right)_{in}^T / \left(\frac{d\sigma}{d\Omega}\right)_{el} = \frac{1}{2} \left(\frac{N}{A}\right)^2 \frac{\omega}{\mu c^2} \frac{(1 + \sin^2 \frac{1}{2}\theta)}{\cos^2 \frac{1}{2}\theta} \quad (67)$$

for the transverse part, where $(d\sigma/d\Omega)_{el}$ is the elastic cross section, N and A are the neutron and mass number, respectively; $\mu = \frac{1}{4}AM$, M being the nucleon mass; ω is the peak energy of the resonance. These expressions are valid under the assumption of $\hbar\omega \ll \epsilon$.

Figure 15 shows the ratio of the transverse and longitudinal cross sections to the elastic one as a function of the momentum transfer. For the longitudinal part this ratio is independent of the angle and depends only on Δ . For the transverse part the ratio is independent of the momentum transfer and depends only on the angle of scattering. Large angles ($\theta \rightarrow 180^\circ$) are more favorable for the observation of the transverse part of the cross section.

Other models were used by Lewis and Walecka⁶⁸ to compute the reduced matrix elements ("inelastic form factors") of the transverse part of the cross section. For the case of C^{12} , which we will discuss here, these were the hydrodynamical model of Steinwedel-Jensen⁷⁸ and the Brown model⁷⁹ (independent-particle model

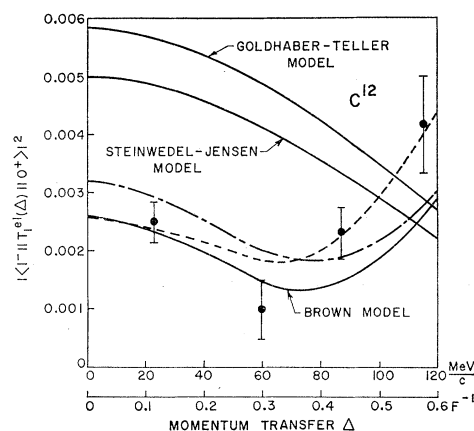


FIG. 16. Inelastic form factor versus momentum transfer for the giant electric-dipole resonance in O^{12} . The solid curve is calculated using a spin-dependent force with zero range for the residual interaction. The dashed curve is calculated using an ordinary force with zero range and leaving the high-lying state in C^{12} out of the calculation. The long-dash short-dash curve is calculated using a Serber force with a Yukawa potential well for the residual interaction. We also show the curves for the collective models and the data of Goldemberg and Barber. But see discussion in Ref. 4.

⁷⁸ H. Steinwedel and J. H. D. Jensen, Z. Naturforsch. **5a**, 413 (1950).

⁷⁹ G. E. Brown and M. Bolsterli, Phys. Rev. Letters **3**, 472 (1959).

with particle-hole interactions). The important result of these calculations is that they give *widely different form factors*, both in absolute magnitude and in their q -dependence. One has, therefore, a sensitive method of testing nuclear models.

Figure 16 shows the "inelastic form factor" for the giant resonance in C^{12} as a function of momentum transfer for the different models. Figure 17 extends the calculations to higher momentum transfers and includes also the longitudinal form factors. The data of Goldemberg and Barber⁸⁰ shown also in these figures are in reasonable agreement with the Brown model. For a more recent discussion of this problem see Ref. 4 and references cited therein.

The choice of the two-particle residual interaction is an important parameter which can affect the results;

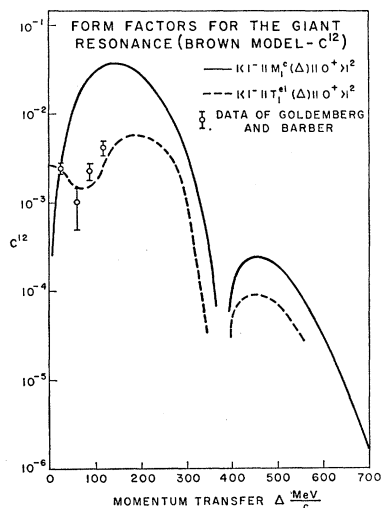


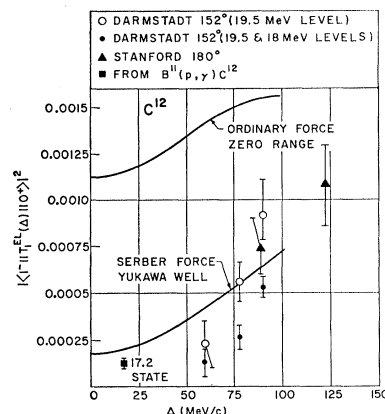
FIG. 17. Longitudinal and transverse form factors versus momentum transfer for the giant dipole resonance in C^{12} . The curves are calculated using a spin-dependent force with zero range for the residual interaction.

in general, one chooses a Serber force with a Yukawa potential well or an ordinary force with zero range. An experimental study of the form factors then gives information on the adequacy of one choice over the other. This was done in detail⁸⁰ for one of the $E1$ levels of C^{12} and Figure 18 shows that a Serber force fits the data considerably better than an ordinary force.

In the independent-particle model the "giant resonance" consists of a number of closely spaced levels which are located in the region of 20-30 MeV below the elastic peak. Each one of these levels corresponds to transitions from the ground state to one of the particle-hole final states; since these may have a different spatial distribution a measurement of the Δ -dependence of the form factors which "probes" this structure might give a result that is typical of each level. This was predicted by Lewis and Walecka⁸¹ and confirmed by experiment; it explains why the shape of

⁸⁰ J. Goldemberg and W. C. Barber, *Phys. Rev.* **134**, B963 (1964).

FIG. 18. Form factor for the lowest 1^- state in C^{12} plotted as a function of the momentum transfer. The two curves are for independent-particle-model calculations with two different assumptions for the two-particle residual interaction.



the giant resonance may be different for photon and for electron scattering excitation.

Figure 19 shows the relative transition probabilities for transverse excitation of the $1^-, T=1$ states of O^{16} .⁸¹ The height of each line is proportional to the square of the form factor corresponding to excitation of that state. The relative magnitudes change with the momentum transfer. Figure 20 shows the experimental data obtained for O^{16} by Burgov *et al.*⁸² (photon absorption) and by Goldemberg and Barber⁸⁰ (for electron excitation at $\hbar\Delta \cong 120$ MeV/c). This shows clearly the inversion in strength of the two main levels at the two momentum transfers. This figure also shows the shell-model calculations of Elliot and Flowers⁸³ for photon excitation in the two main levels of O^{16} .

A considerable amount of detailed, high-resolution work of this type remains to be done; it is expected that

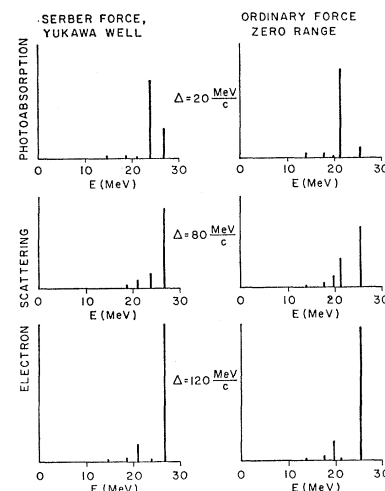


FIG. 19. Relative transition probabilities for transverse excitation of the $1^-, T=1$ states in O^{16} . The height of each line is proportional to the square of the form factor for excitation of the corresponding state at the given energy and momentum transfer. Two types of residual interaction were used.

⁸¹ F. H. Lewis, *Phys. Rev.* **134**, B331 (1964).

⁸² N. A. Burgov, G. V. Danilyan, B. S. Dolbilkin, E. Lazareva, and F. A. Nikolaev, *Zh. Eksperim. i Teor. Fiz.* **43**, 70 (1962) [English transl.: *Soviet Phys.—JETP* **16**, 50 (1963)].

⁸³ J. P. Elliot and B. H. Flowers, *Proc. Roy. Soc. (London)* **242A**, 57 (1957).

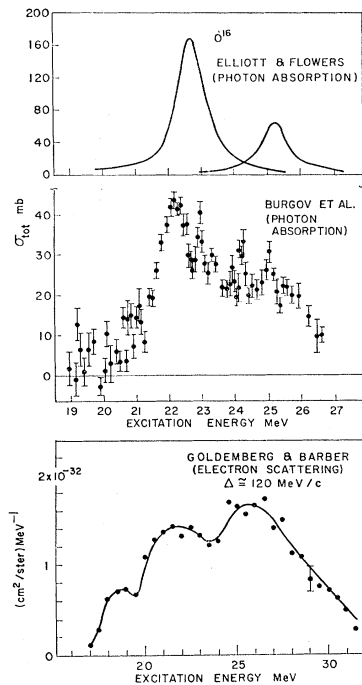


FIG. 20. A comparison of the photon-absorption cross-section measurements of Burgov *et al.* in O^{16} with the electron scattering cross-section measurements of Goldemberg and Barber at a Δ of 120 MeV/c and 180°. The top graph shows the results of the calculation of Elliott and Flowers.

inelastic electron scattering in levels will prove to be an important tool for nuclear structure studies. Experimental⁸⁴ and theoretical⁸⁵ studies are proceeding rapidly.

D. Quasielastic (Incoherent) Scattering

Extending the measurement of inelastic scattered electrons to include large energy losses, one finds the region of "quasielastic" scattering ("d" in Fig. 4). The reason for the name is related to the analogous process of Compton scattering of x rays by bound electrons; if one measures the scattered x rays at a given angle one finds a modified Compton line. In the case of high-energy incident electrons the modified line (scattered electrons) is found in a position determined by the binding energy of the nucleus and the recoil in the electron-nucleon interaction. In addition however the nucleons are moving with high energies inside the nucleus; consequently the scattered electrons are spread out in energies, the spreading being determined by the momentum distribution of the nucleons. Each individual nucleon gives a spread-out contribution to the inelastic scattering and the superposition of all of them constitutes the quasielastic or "incoherent" peak.

The relation between the shape and integrated area of this broad peak and the momentum distribution of the nucleons has been studied extensively by Drell and

Schwartz,⁸⁶ McVoy and van Hove,⁸⁷ Gottfried and Czyz,⁸⁸ and recently Czyz.⁸⁹ These calculations show that the main part of the quasielastic peak is determined by the Pauli principle correlations and the results are rather model insensitive, to the point that even a free degenerate Fermi gas gives roughly the right shape and position.

Figure 21 shows measurements of Leiss and Taylor,⁹⁰ with 148.5-MeV incident electrons at 135° in C^{12} , and the calculations of Czyz considering all single-particle excitations compatible with the Pauli principle. The momentum distribution for the C^{12} nucleus was taken as

$$n(p) = [1 + \frac{4}{3}(p/p_0)^2] \exp[-(p/p_0)^2]. \quad (68)$$

Several values of the effective mass M_{eff} of the nucleons inside nuclear matter were tried. Agreement between theory and experiment is reasonable. Other data for C^{12} at higher energies is reported by Bounin and Bishop.⁹¹

The high-energy tail of the quasielastic peak is determined by short-range nucleon-nucleon dynamical correlations, which are the most interesting to study; it is located however in a place where experiments are difficult. Kendall and Isabelle⁹² obtained some information of this kind. The high-energy tail contributes little to the total area under the peak; the calculated sum-rules are insensitive to details of the correlations. Furthermore the radiation tail over the extended region of the quasielastic region cannot be obtained with high accuracy.⁹¹

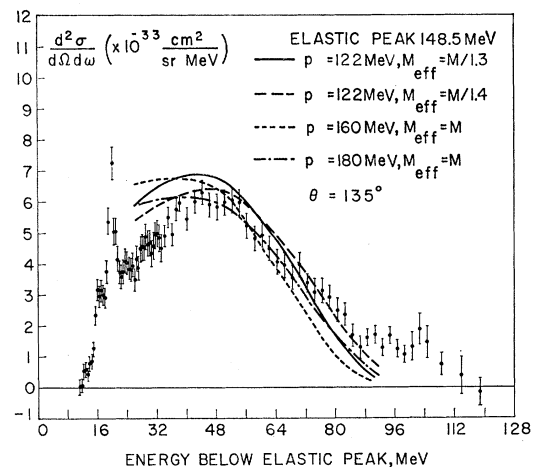


FIG. 21. Comparison of impulse approximation calculations for C^{12} with measurements of Leiss and Taylor. The energy of the incident electrons is 148.5 MeV and the spectrum was measured at 135°.

⁸⁶ S. D. Drell and C. L. Schwartz, Phys. Rev. **112**, 568 (1958).

⁸⁷ K. W. McVoy and L. Van Hove, Phys. Rev. **125**, 1034 (1962).

⁸⁸ W. Czyz and K. Gottfried, Ann. Phys. (N.Y.) **21**, 47 (1963).

⁸⁹ W. Czyz, Phys. Rev. **131**, 2141 (1963).

⁹⁰ J. E. Leiss and R. E. Taylor (quoted in Ref. 66).

⁹¹ J. I. Friedman, Phys. Rev. **116**, 1257 (1959); P. Bounin and G. R. Bishop, J. Phys. Radium **29**, 974 (1963).

⁹² D. B. Isabelle and H. W. Kendall, Bull. Am. Phys. Soc. **9**, 95 (1964).

⁸⁴ G. Vanpraet, Phys. Letters **17**, 120 (1965); G. Vanpraet, Nucl. Phys. **74**, 219 (1965); G. J. Vanpraet, W. C. Barber, P. Kessanyi-Demay, and G. J. Vanpraet (to be published).

⁸⁵ T. deForest Phys. Rev. **139**, B1217 (1965); T. deForest, J. D. Walecka, G. Vanpraet, and W. C. Barber, Phys. Letters **16**, 311 (1965); J. L. Friar (to be published).

However it has been pointed out recently by Czyz⁹³ that an interesting case occurs at very large angles ($\theta \sim 180^\circ$). The sum-rule of McVoy and van Hove⁸⁷ is

$$\int_0^\infty \frac{d\sigma}{d\omega d\Omega}(\Delta, \omega, \theta) d\omega = |f(\Delta)|^2 \left(\frac{e}{2p_1}\right) \frac{\cos^2 \frac{1}{2}\theta}{\sin^2 \frac{1}{2}\theta} [A(\Delta) + B(\Delta) + \tan^2 \frac{1}{2}\theta], \quad (69)$$

where ω is the energy loss of the electrons. $f(\Delta)$ is related to the conventional form factors by

$$f(\Delta) = F_{1p}(\Delta) = F_{2p}(\Delta) = F_{2n}(\Delta); \quad F_{1n}(\Delta) \text{ (assumed zero)}. \quad (70)$$

At 180° one can measure $B(\Delta)$, which is given (to second order in Δ/M) by

$$B(\Delta) = (\Delta^2/M^2) (Z^2\mu_p^2 + N^2\mu_n^2) + \frac{4}{3}Z \langle \langle p^2 \rangle_n / M^2 \rangle + \langle 0 | \sum_{j \neq k}^A \sum_{k=1}^A \exp [i\Delta \cdot (\mathbf{r}_j - \mathbf{r}_k)] \{ \mu_j \mu_k (2M^2)^{-1} [\Delta^2 \delta_j \cdot \delta_k - (\Delta \cdot \delta_j)(\Delta \cdot \delta_k)] + \mu e_j e_k (p_{xj} p_{xk} / M^2) \} | 0 \rangle, \quad (71)$$

where Z and N are the number of protons and neutrons, μ_p and μ_n their magnetic moments *inside* nuclear matter, $e_j = 1$ for protons and 0 for neutrons; δ_j are spin operators; p_{xj} is the component of \mathbf{p}_j in a direction normal to Δ . The summation extends over all nucleons.

The first term of $B(\Delta)$ is the dominant one (for $\Delta = 1$ F) it makes up 90% of the total) and becomes more dominant as Δ increases. The others can be evaluated with an accuracy of perhaps 25% and although model-sensitive do not contribute much in the result. Consequently a precise measurement of $B(\Delta)$ could be important in establishing the equality of the magnetic moments inside nuclear matter with their values for the free nucleons; it seems feasible in this way to find out about the "quenching" of magnetic moments inside the nucleus.⁹⁴

The electrodisintegration of the deuteron is an important special problem of the type discussed in this section. Calculations have been made using well-known wave functions due to Yankus.⁹⁵ The deuteron has no bound excited states and it disintegrates at 2.23 MeV so there are no levels in the spectrum but only a broad peak that extends down to lower energies. Measurements have been made at forward angles by many authors.^{1,2} Peterson and Barber²¹ and Barber *et al.*¹⁸ measured the spectrum of electrons inelastically scattered from the

deuteron at 180° using 41.5-MeV electrons and compared their results with the Yankus theory,⁹⁵ neglecting exchange currents. All multipole order transitions were taken into account although the magnetic dipole ($M1$) process is predominant; final-state interactions were not taken into account. Agreement with theory was obtained with little evidence for effects due to exchange currents although they are expected to contribute. These experiments have been recently extended to higher energies by Goldemberg and Schaerf⁹⁶ and some disagreement with theory is apparent from the data.

ACKNOWLEDGMENTS

We are pleased to acknowledge useful discussions with Professor W. C. Barber, Professor J. D. Walecka, Dr. F. H. Lewis, Dr. E. Ginsberg, Dr. W. Czyz, and Professor S. D. Drell. This review was begun at Stanford University and supported in part by the U.S. Air Force through Air Force Office of Scientific Research Contract AF 49(638)-1389, and in part by the joint program of the U.S. Office of Naval Research, the Atomic Energy Commission, and the U.S. Air Force Office of Scientific Research. We wish to thank Professor L. I. Schiff and Professor W. C. Barber for the hospitality extended to us in the Physics Department and the High Energy Physics Laboratory at Stanford University.

⁹³ W. Czyz (private communication).

⁹⁴ B. Bremond, *Nucl. Phys.* **35**, 49 (1962).

⁹⁵ V. Z. Jankus, *Phys. Rev.* **102**, 1586 (1956).

⁹⁶ C. Schaerf and J. Goldemberg (to be published).